

Supporting Information (SI) for:

Asymmetric 1,3-dipolar cycloaddition reaction of chiral 1-alkyl-1,2-diphospholes with diphenyldiazomethane

Yulia Ganushevich,^a Almaz Zagidullin,^a Svetlana Kondrashova,^a Shamil Latypov,^a Vasili Miluykov,^a Peter Lönnecke,^b Evamarie Hey-Hawkins^b

^a*Arbuzov Institute of Organic and Physical Chemistry, FRC Kazan Scientific Center of RAS, 420088, Kazan, Russia, almaz.zagidullin@gmail.com*

^b*Institute of Inorganic Chemistry, Leipzig University, 04103, Leipzig, Germany*

Table of contents

pages

Calculation details	S3
Table S1. Energies (PBE0/6-31+G(d)) of main forms due to rotation around P2-CH ₂ bond in the model of compound 3 (3' , methyl instead of menthyl).	S4
Figure S1. The major form of the model compound 3' (methyl instead of menthyl): front and side views.	S4
Table S2. Energies (PBE0/6-31+G(d)) and some key ¹³ C and ³¹ P NMR chemical shifts (GIAO PBE0/6-31+G(d)//PBE0/6-311G(2d,2p)) calculated for 3a and 3b	S4
Figure S2. High field sections of the ¹ H NMR spectra of 3a (a, b) and 3b (c, d) in CDCl ₃ at room and low temperatures.	S5
Table S3. Energies (PBE0/6-31+G(d)) and some key ¹³ C and ³¹ P NMR chemical shifts (GIAO PBE0/6-31+G(d)//PBE0/6-311G(2d,2p)) calculated for 5a and 5b	S6
Figure S3. Structures of isomers 5a (a) and 5b (b) with indicative NMR effects.	S6
Figure S4. 1D ¹ H and ³¹ P{ ¹ H} NMR spectra of 3a in CDCl ₃ at T = 303 K.	S7
Figure S5. 2D ¹ H- ³¹ P HMBC NMR spectrum of 3a in CDCl ₃ at T = 303 K.	S8
Figure S6. 1D ¹ H, ¹³ C DEPT and ¹³ C{ ¹ H} NMR spectra of 3a in CDCl ₃ at T = 303 K.	S9
Figure S7. 2D ¹ H- ¹ H COSY NMR spectrum of 3a in CDCl ₃ at T = 303 K.	S10
Figure S8. 2D ¹ H- ¹ H COSY NMR spectrum of 3a in CDCl ₃ at T = 233 K.	S11
Figure S9. 2D ¹ H- ¹³ C HSQC NMR spectrum of 3a in CDCl ₃ at T = 303 K.	S12
Figure S10. 2D ¹ H- ¹³ C HMBC NMR spectrum of 3a in CDCl ₃ at T = 303 K.	S13
Figure S11. 1D ¹ H and ¹ H NOESY NMR spectra of 3a in CDCl ₃ at T = 303 K.	S14
Figure S12. 1D ¹ H and ³¹ P{ ¹ H} NMR spectra of 3b in CDCl ₃ at T = 303 K.	S15

Figure S13. 2D ^1H - ^{31}P HMBC NMR spectrum of 3b in CDCl_3 at $T = 303\text{ K}$.	S16
Figure S14. 1D ^1H , ^{13}C DEPT and $^{13}\text{C}\{^1\text{H}\}$ NMR spectra of 3b in CDCl_3 at $T = 303\text{ K}$.	S17
Figure S15. 2D ^1H - ^1H COSY NMR spectrum of 3b in CDCl_3 at $T = 303\text{ K}$.	S18
Figure S16. 2D ^1H - ^1H COSY NMR spectrum of 3b in CDCl_3 at $T = 233\text{ K}$.	S19
Figure S17. 2D ^1H - ^{13}C HSQC NMR spectrum of 3b in CDCl_3 at $T = 303\text{ K}$.	S20
Figure S18. 2D ^1H - ^{13}C HMBC NMR spectrum of 3b in CDCl_3 at $T = 303\text{ K}$.	S21
Figure S19. 1D ^1H and ^1H NOESY NMR spectra of 3b in CDCl_3 at $T = 303\text{ K}$.	S22
Figure S20. 1D ^1H and ^1H NOESY NMR spectra of 3b in CDCl_3 at $T = 303\text{ K}$.	S23
Figure S21. 1D ^1H and $^{31}\text{P}\{^1\text{H}\}$ NMR spectra of 5a and 5b in CDCl_3 at $T = 303\text{ K}$.	S24
Figure S22. 2D ^1H - ^{31}P HMBC NMR spectrum of 5a and 5b in CDCl_3 at $T = 303\text{ K}$.	S25
Figure S23. 1D ^1H , ^{13}C DEPT and $^{13}\text{C}\{^1\text{H}\}$ NMR spectra of 5a and 5b in CDCl_3 at $T = 303\text{ K}$.	S26
Figure S24. 2D ^1H - ^1H COSY NMR spectrum of 5a and 5b in CDCl_3 at $T = 303\text{ K}$.	S27
Figure S25. 2D ^1H - ^{13}C HSQC NMR spectrum of 5a and 5b in CDCl_3 at $T = 303\text{ K}$.	S28
Figure S26. 2D ^1H - ^{13}C HMBC NMR spectrum of 5a and 5b in CDCl_3 at $T = 303\text{ K}$.	S29
Figure S27. 1D ^1H and ^1H NOESY NMR spectra of 5a and 5b in CDCl_3 at $T = 303\text{ K}$.	S30
Figure S28. 1D ^1H and ^1H NOESY NMR spectra of 5a and 5b in CDCl_3 at $T = 303\text{ K}$.	S31
Figure S29. 1D ^1H and ^1H NOESY NMR spectra of 5a and 5b in CDCl_3 at $T = 303\text{ K}$.	S32
Figure S30. 1D ^1H and ^1H TOCSY NMR spectra of 5a and 5b in CDCl_3 at $T = 303\text{ K}$.	S33
Table S4. Basic crystallographic structure parameters for 5a .	S34
Figure S31. Molecular structure of 5a .	S35
Figure S32. Thermal ellipsoid plot (50% probability level) for the crystal structure of 5a .	S36
References.	S37

Calculation details

The quantum chemical calculations were performed with the Gaussian 03 software package.¹ Full geometry optimizations have been carried out within the framework of DFT (PBE0) method using 6-31+G(d) basis sets. Chemical shifts were calculated at the PBE0/6-311G(2d,2p) level of theory. ¹³C chemical shifts were referred to TMS. ³¹P chemical shifts were referred to H₃PO₄, and a linear scaling procedure was applied.²

References: see S37

Details of structure elucidation by NMR

The structures of compounds **3a**, **3b** and **5a** were established by verity of 1D/2D NMR correlation methods. Namely, starting from the group with well known “finger prints” structure of whole compound can be established practically directly.

For example, for **3a** we can start from the P2-CH₂O protons with characteristic ABXY type spin system (at 3.95 and 3.62 ppm).

As to the menthyl fragment: There is ¹H-¹³C HMBC correlation from the P2-CH₂O protons to C1' (80.52 ppm). Then from ¹H-¹³C HSQC experiment the H1' (3.01 ppm) proton can be established. Next there are ¹H-¹³C HMBC connectivity's from the H1' proton to C2' (48.91 ppm), to C5' (31.56 ppm), to C7' (24.76 ppm) and to P2-CH₂O (64.79 ppm) carbons. There are also NOE's from the P2-CH₂O protons to H1', to H6eq' and to H7' protons. Then combination of ¹H-¹H COSY, ¹H-¹³C HSQC and ¹H-¹³C HMBC experiments allows to assign all signals in ¹H and ¹³C spectra of the menthyl moiety. The most important connectivity's are from H7' to Me-8' and Me-9' (¹H-¹H COSY and ¹H-¹³C HMBC); and from H5' to Me-10' (¹H-¹H COSY and ¹H-¹³C HMBC).

As to the bicyclic phosphirane fragment: There are ¹H-³¹P HMBC correlations from the P2-CH₂O protons to P1 (-121.4 ppm) and to P2 (6.2 ppm). There is also ¹H-¹³C HMBC connectivity from the P2-CH₂O protons to C3 (144.52 ppm). ¹³C DEPT experiments help to distinguish protonated carbons from not protonated ones (CH *versus* C) in low field region. Then, four less intense signals of protonated carbons can be assigned to *para*-carbons of phenyl rings. Doublets in low field region of the ¹H spectra are due to *ortho*-protons. Then there is correlation from the *o*-Ph3 (d, 6.3 ppm) protons to C3 (¹H-¹³C HMBC), to P2 (¹H-³¹P HMBC) and to the P2-CH₂O protons (NOE). There are correlations from the *o*-Ph6 (d, 7.65 ppm) and the *o*-Ph6' (d, 6.9 ppm) protons to C6 (54.09 ppm, ¹H-¹³C HMBC) and P1 (¹H-³¹P HMBC). The *o*-Ph6 *versus* *o*-Ph6' protons can be distinguished upon NOE between the *o*-Ph6 and the *o*-Ph3 protons. There is also NOE between the *o*-Ph3 and the *o*-Ph4 protons. There is ¹H-¹³C HMBC correlation from the *o*-Ph4 protons to C4 (151.12 ppm). Unfortunately, there is no ¹H-¹³C HMBC connectivity's to C5 (73.08 ppm) due to: 1) the *o*-Ph5 protons are broadened due to sterical hindrance; 2) there is no other protons in close proximity. But it's characteristic chemical shift and ¹JCP (37.8 Hz) allows assign the signal to C5. This is also in good agreement with results of calculations. Finally, starting from the ortho-protons all other signals in ¹³C and ¹H spectra can be well assigned upon ¹H-¹³C HMBC, ¹H-¹³C HSQC and ¹H-¹H COSY connectivity's.

In similar way structures of **3b** and **5a** were established.

In the case of compound **5b** the bicyclic phosphirane fragment signals in ¹H and ¹³C NMR spectra cannot be resolved (except C4-*o*-Ph and C3-*o*-Ph) due to intensive overlap with the main isomer (**5a**) signals therefore only the data for the neomenthyl fragment is given. In this case ¹H-³¹P HMBC, ¹H-¹H COSY and ¹H-¹³C HSQC spectra are particularly helpful. The ¹H-³¹P HMBC spectra allows to reveal the protons coupled with minor phosphorus signals, while the ¹H-¹H COSY and ¹H-¹³C HSQC spectra helps to resolve ¹H and ¹³C signals of neomenthyl fragment. But no information about exact multiplet structure of the ¹H and ¹³C spectra can be obtained in this way for some of the protons.

Table S1. Energies (PBE0/6-31+G(d)) of main forms due to rotation around P2-CH₂ bond in the model of compound **3** (**3'**, methyl instead of menthyl).

Energy	-g*	trans	+g
hartree	-2145.8153312	-2145.8190703	-2145.8169151
kcal/mol	2.3	0	1.4

* orientation with respect to the lone pair of electrons at phosphorus, C-O with lone pair of electrons; "+" – clockwise;

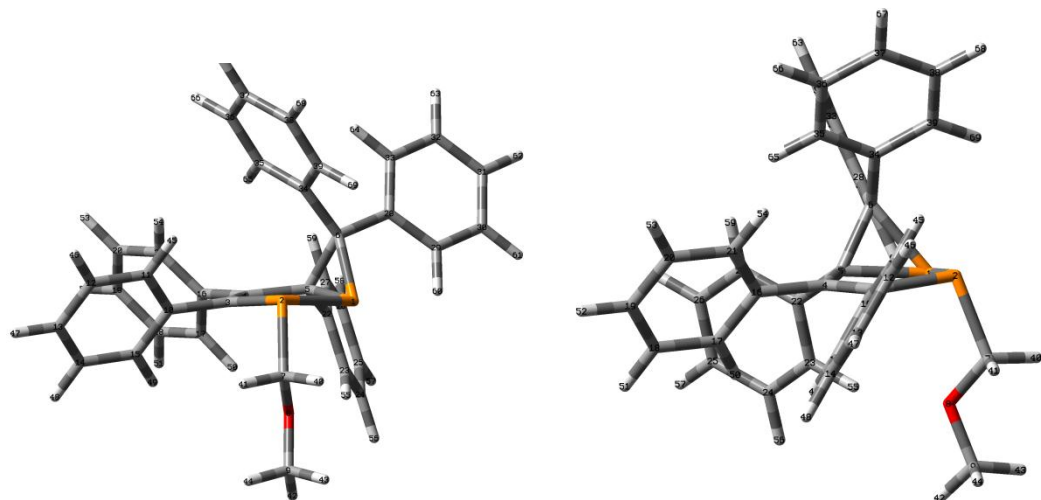


Figure S1. The major form of the model compound **3'** (methyl instead of menthyl): front and side views.

Table S2. Energies (PBE0/6-31+G(d)) and some key ¹³C and ³¹P NMR chemical shifts (GIAO PBE0/6-31+G(d)//PBE0/6-311G(2d,2p)) calculated for **3a** and **3b**.

	3a	3b
Energy, hartree	-2498.0263604	-2498.026385
Energy, kcal/mol	0.015	0
P1	-105.7	-102.4
P2	13.6	16.1
C3	156.0	156.9
C4	158.5	157.7
C5	80.3	80.3
C6	58.2	58.4

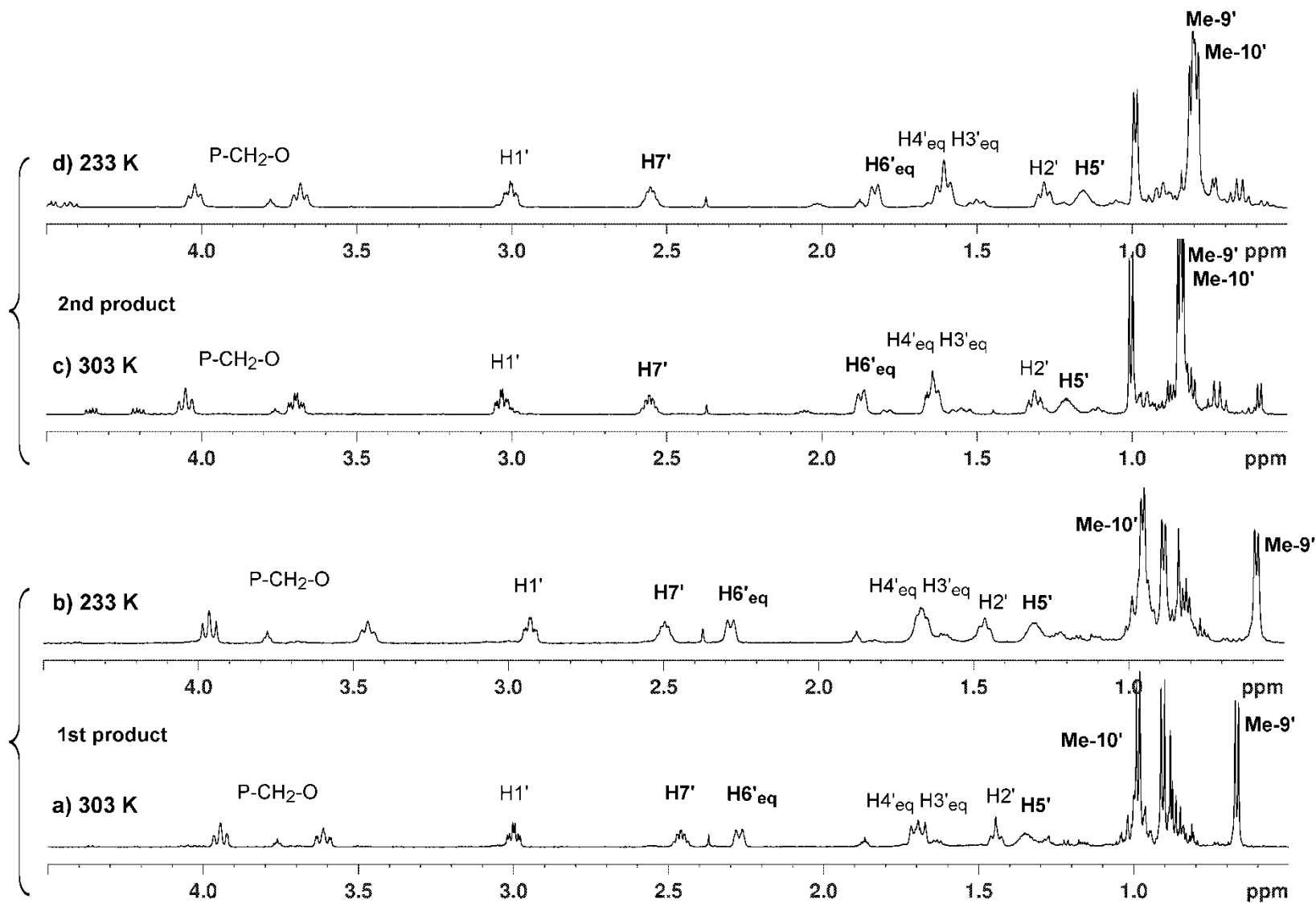


Figure S2. High field sections of the ^1H NMR spectra of **3a** (a, b) and **3b** (c, d) in CDCl_3 at room and low temperatures.

Table S3. Energies (PBE0/6-31+G(d)) and some key ^{13}C and ^{31}P NMR chemical shifts (GIAO PBE0/6-31+G(d)//PBE0/6-311G(2d,2p)) calculated for **5a** and **5b**.

	5a	5b
Energy,	-2383.6206784	-2383.6181352
Energy, kcal/mol	0	1.6
P1	-85.7	-104.7
P2	22.3	15.5
C3	159.5	155.6
C4	156.8	159.5
C5	82.7	80.8
C6	60.0	58.0

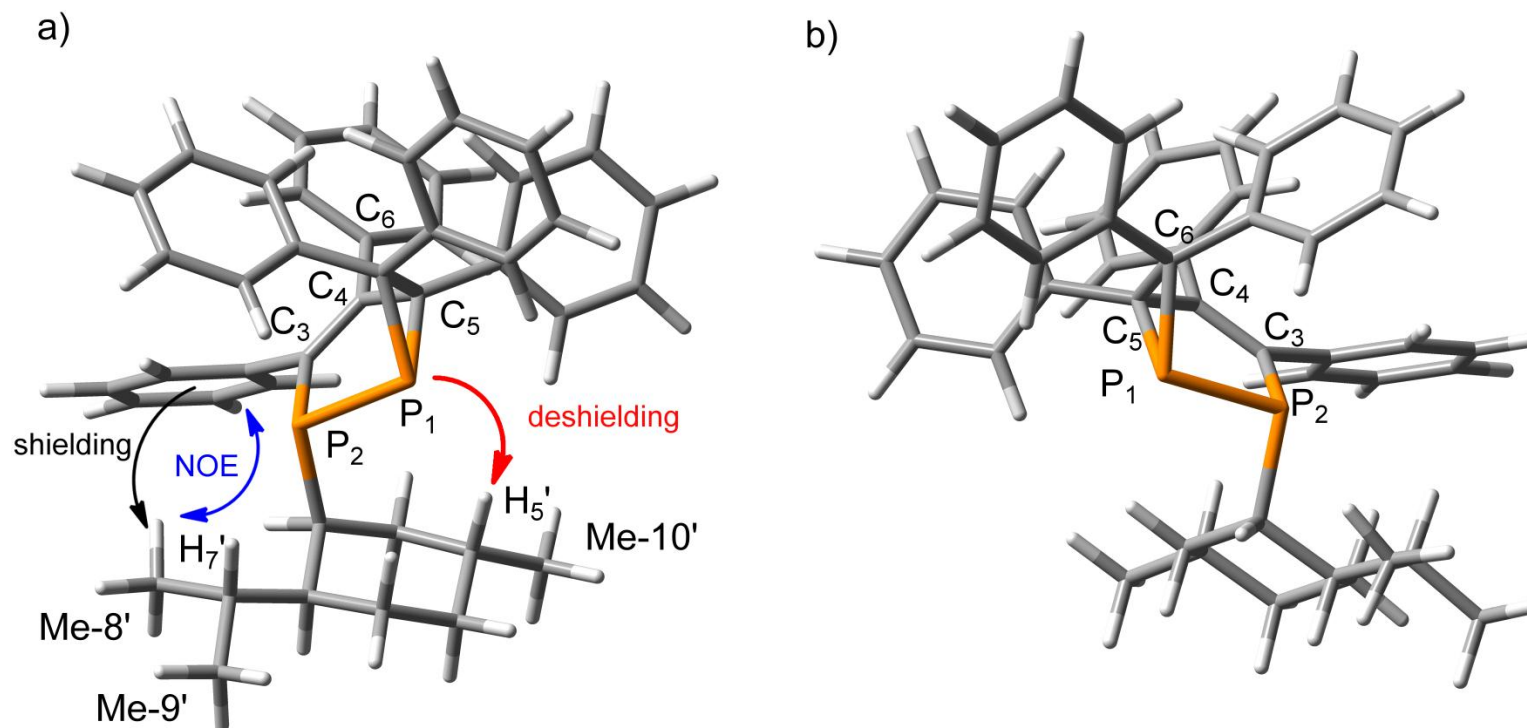


Figure S3. Structures of isomers **5a** (a) and **5b** (b) with indicative NMR effects.

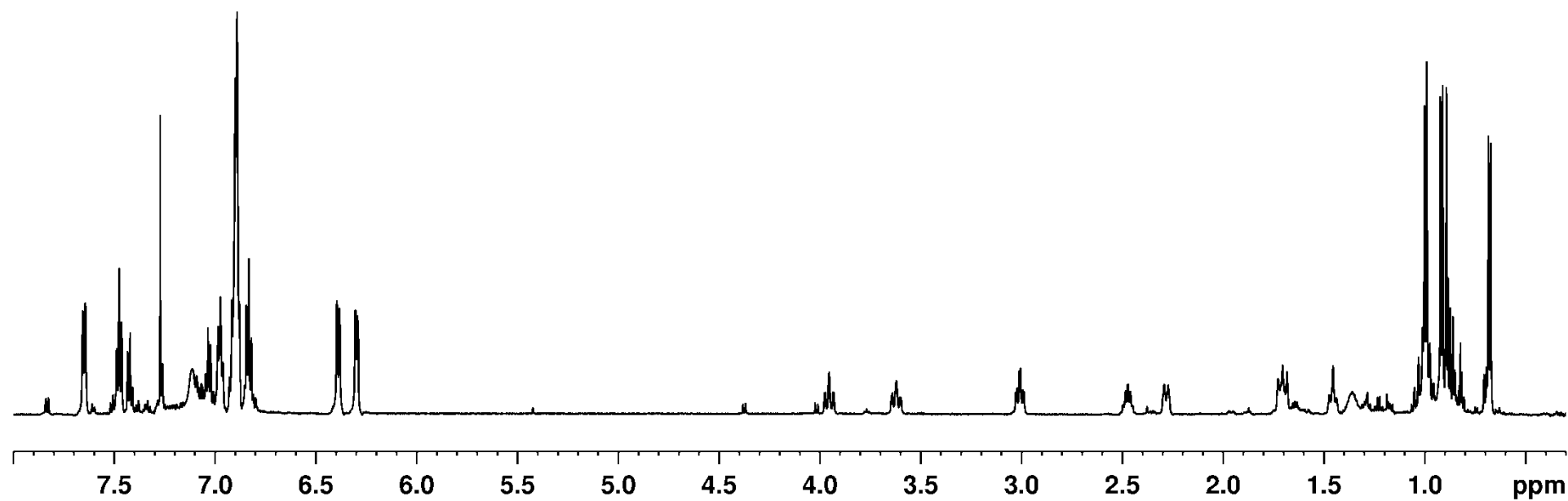
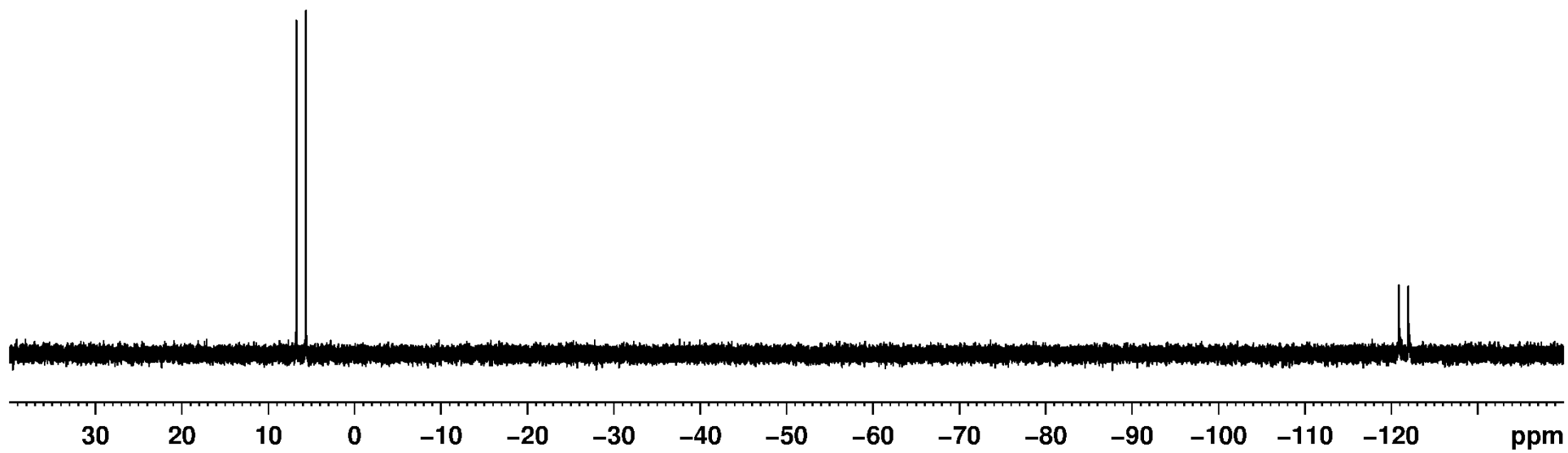


Figure S4. 1D ^1H and $^{31}\text{P}\{^1\text{H}\}$ NMR spectra of **3a** in CDCl_3 at $T = 303$ K.

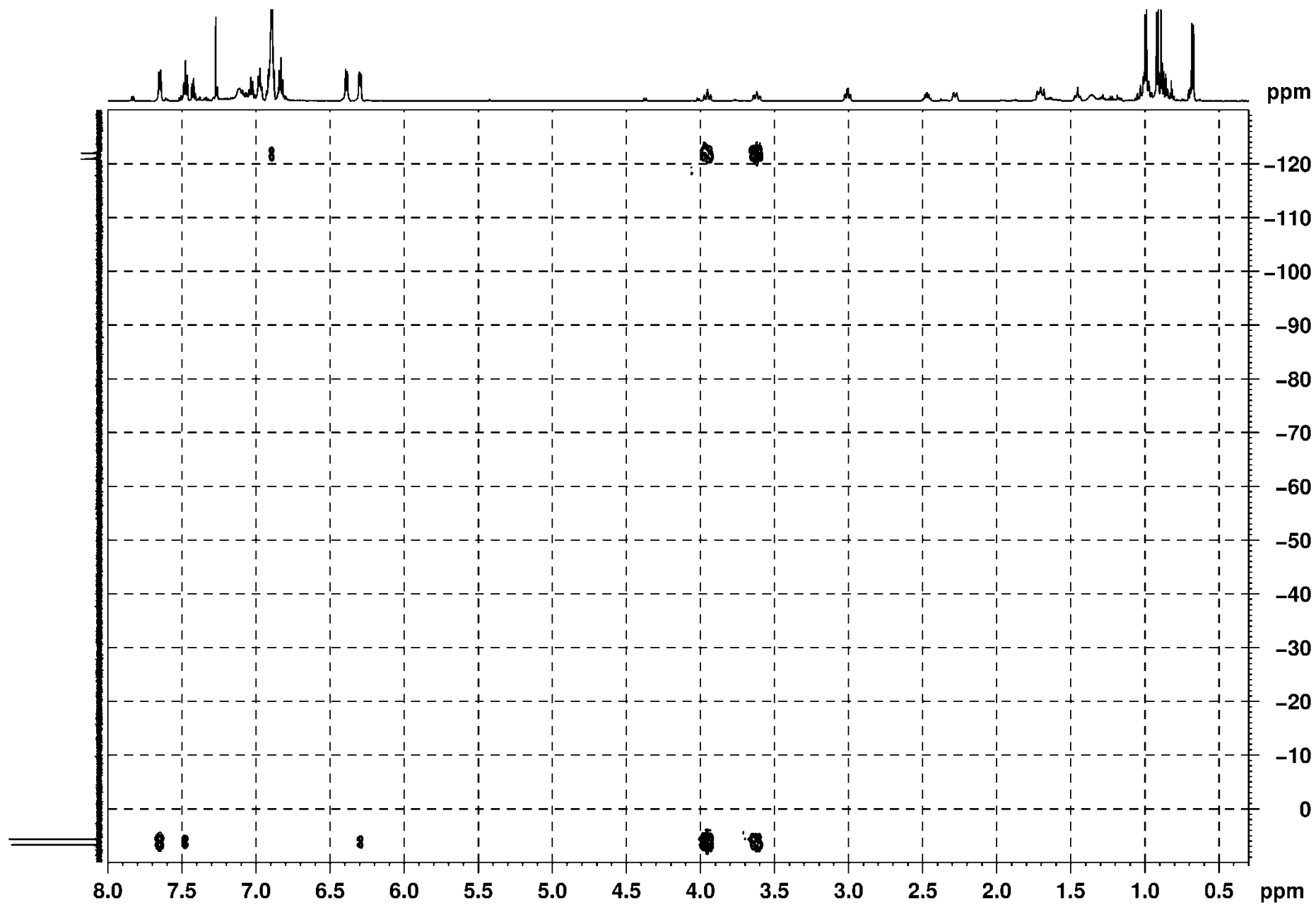


Figure S5. 2D ^1H - ^{31}P HMBC NMR spectrum of **3a** in CDCl_3 at $T = 303$ K.

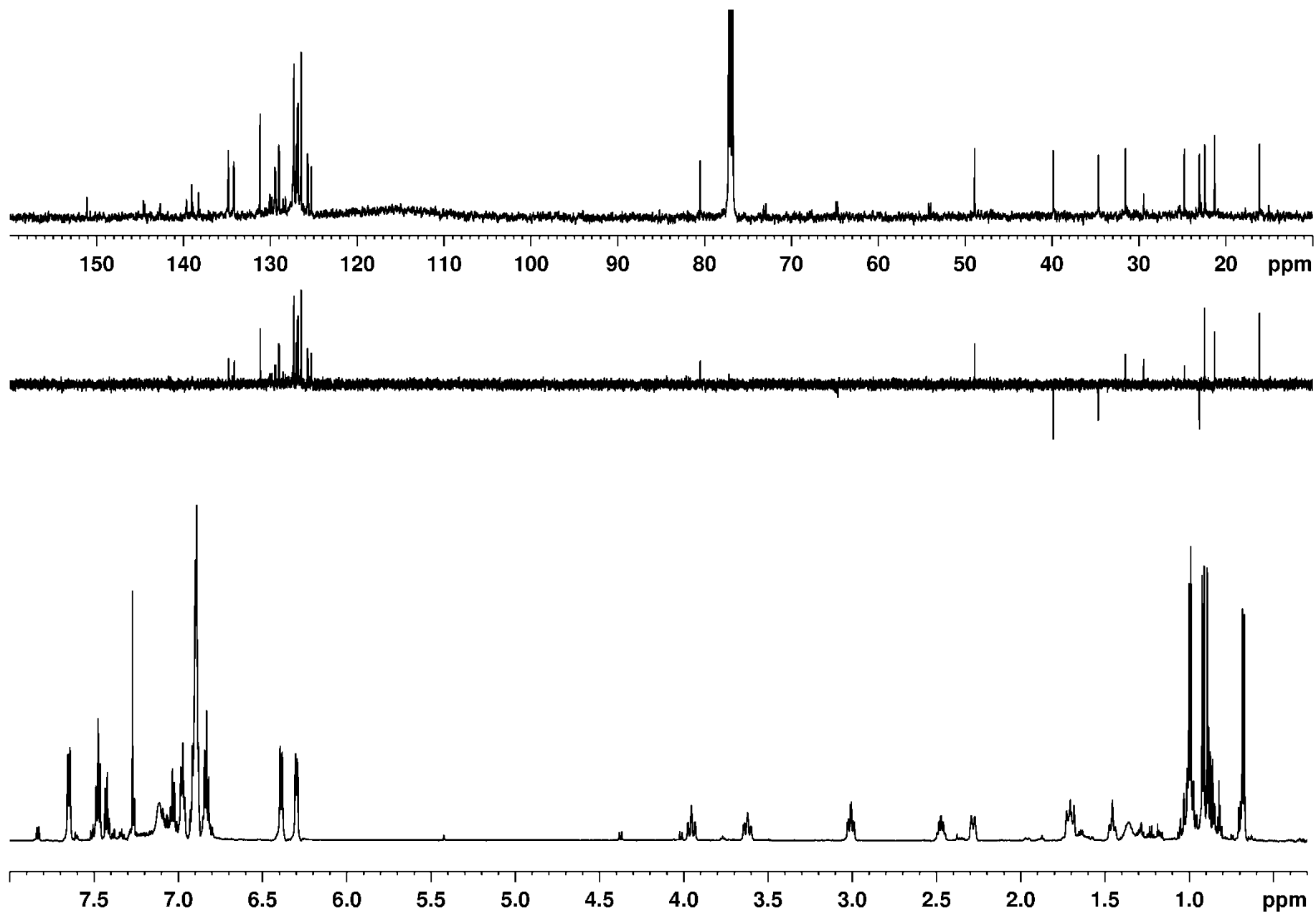


Figure S6. 1D ¹H, ¹³C DEPT and ¹³C{¹H} NMR spectra of **3a** in CDCl₃ at T = 303 K.

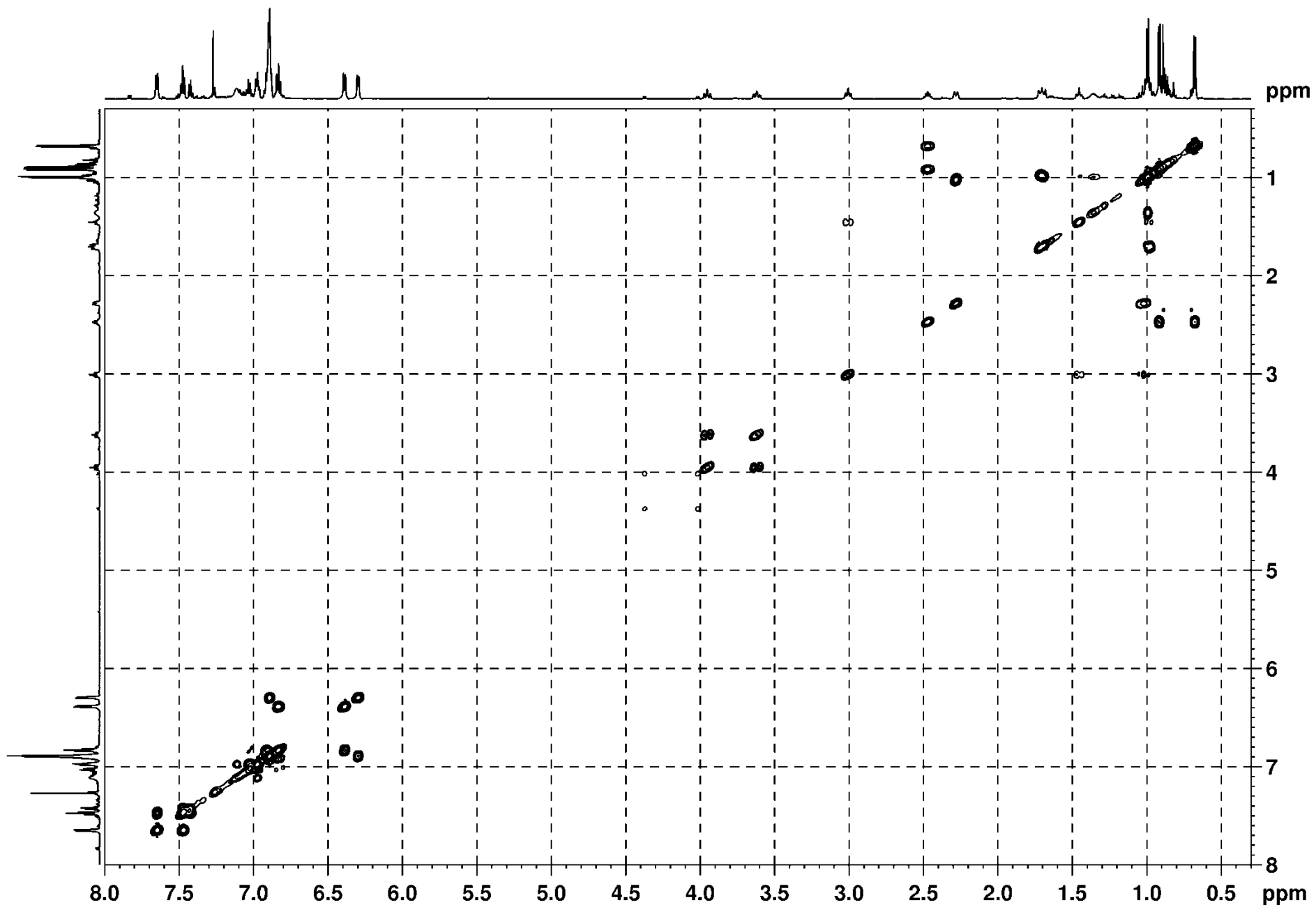


Figure S7. 2D ^1H - ^1H COSY NMR spectrum of **3a** in CDCl_3 at $T = 303$ K.

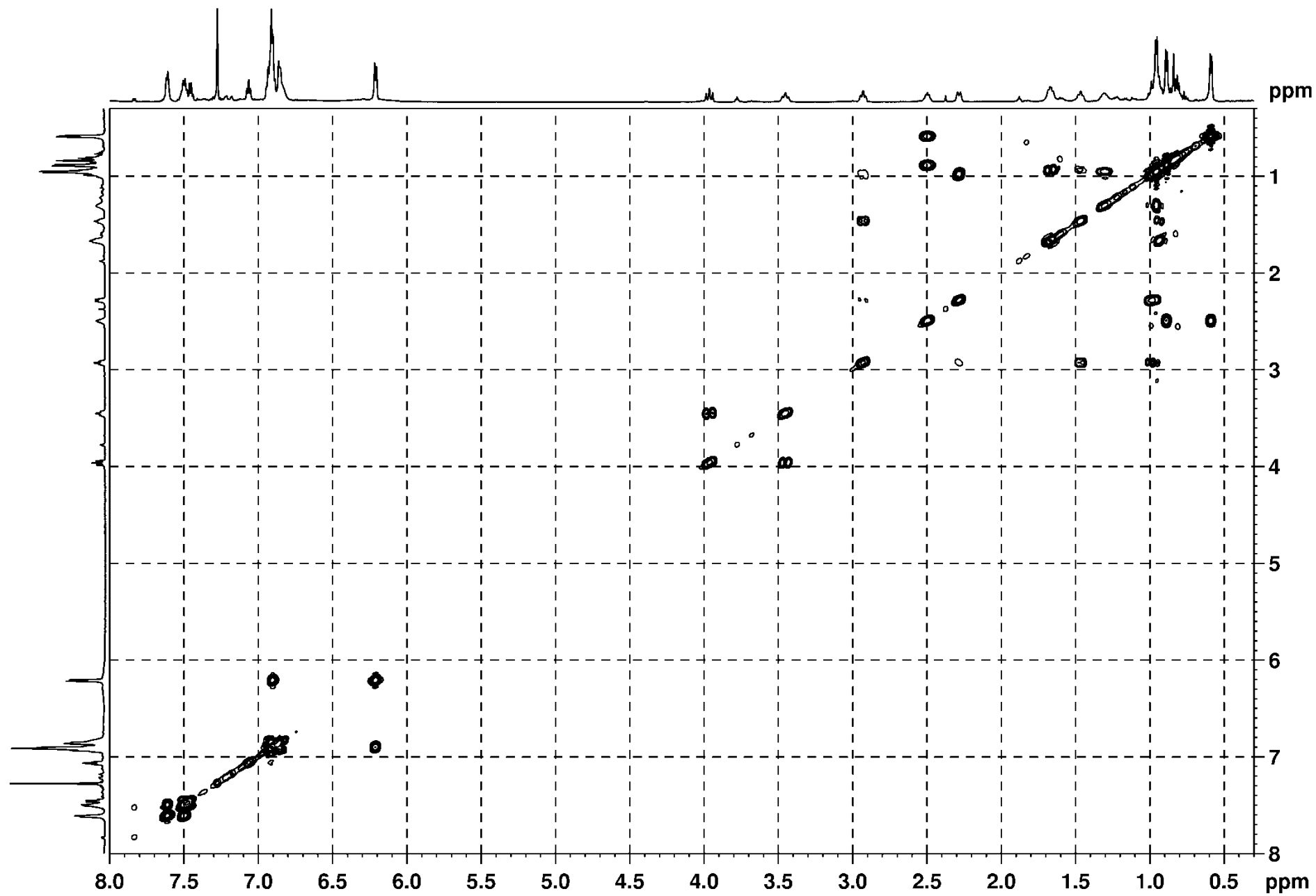


Figure S8. 2D ^1H - ^1H COSY NMR spectrum of **3a** in CDCl_3 at $T = 233\text{ K}$.

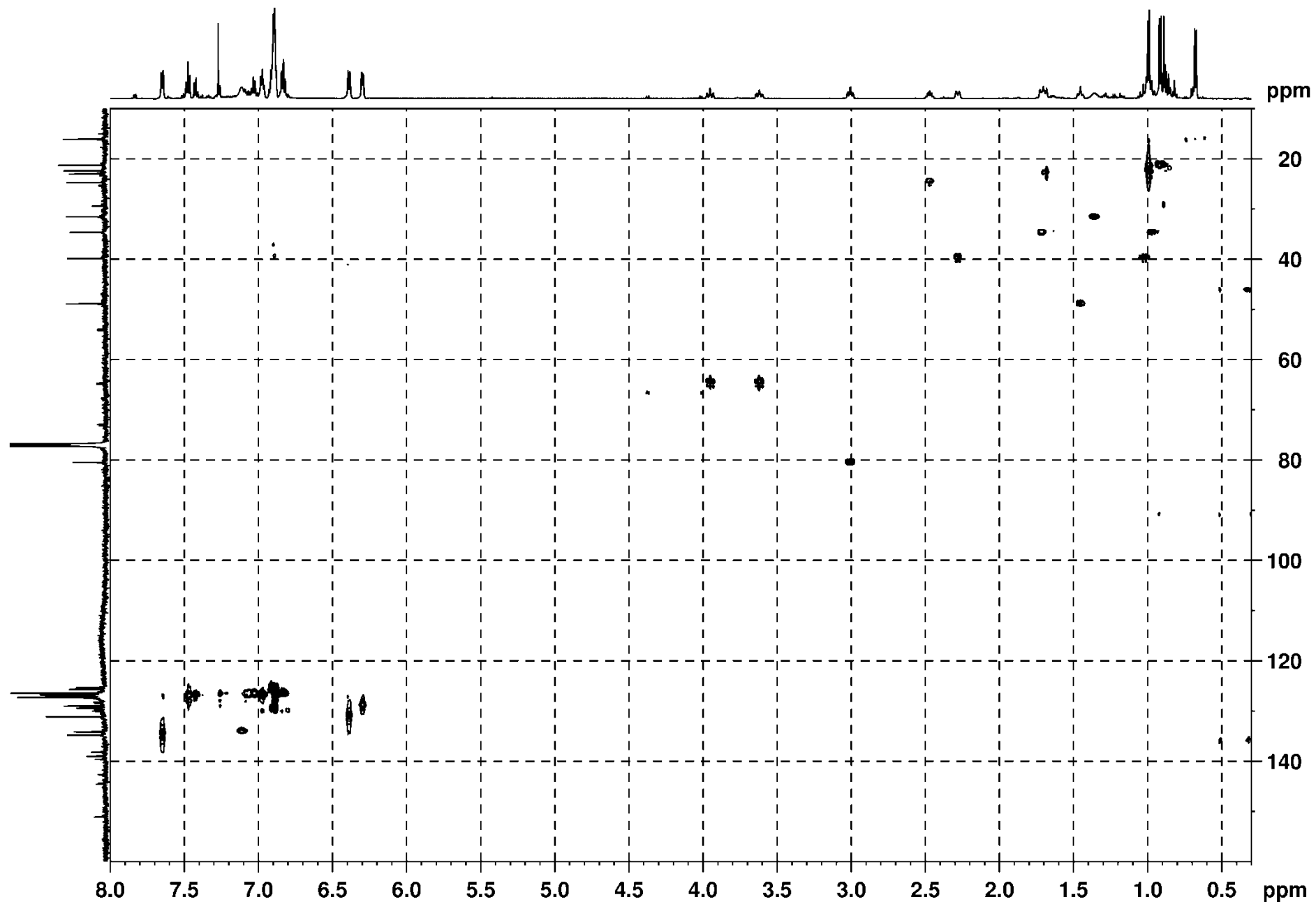


Figure S9. 2D ^1H - ^{13}C HSQC NMR spectrum of **3a** in CDCl_3 at $T = 303$ K.

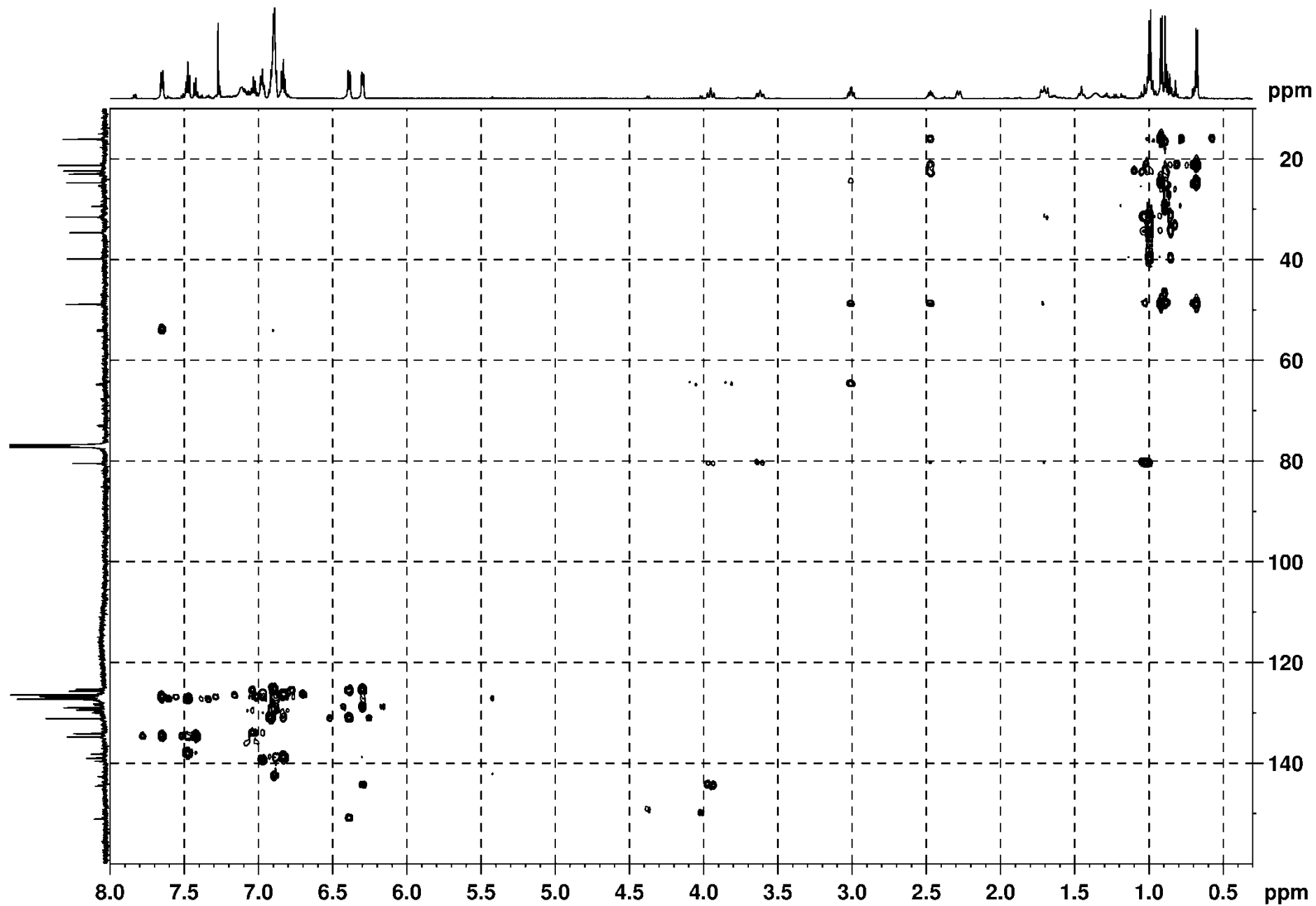


Figure S10. 2D ^1H - ^{13}C HMBC NMR spectrum of **3a** in CDCl_3 at $T = 303$ K.

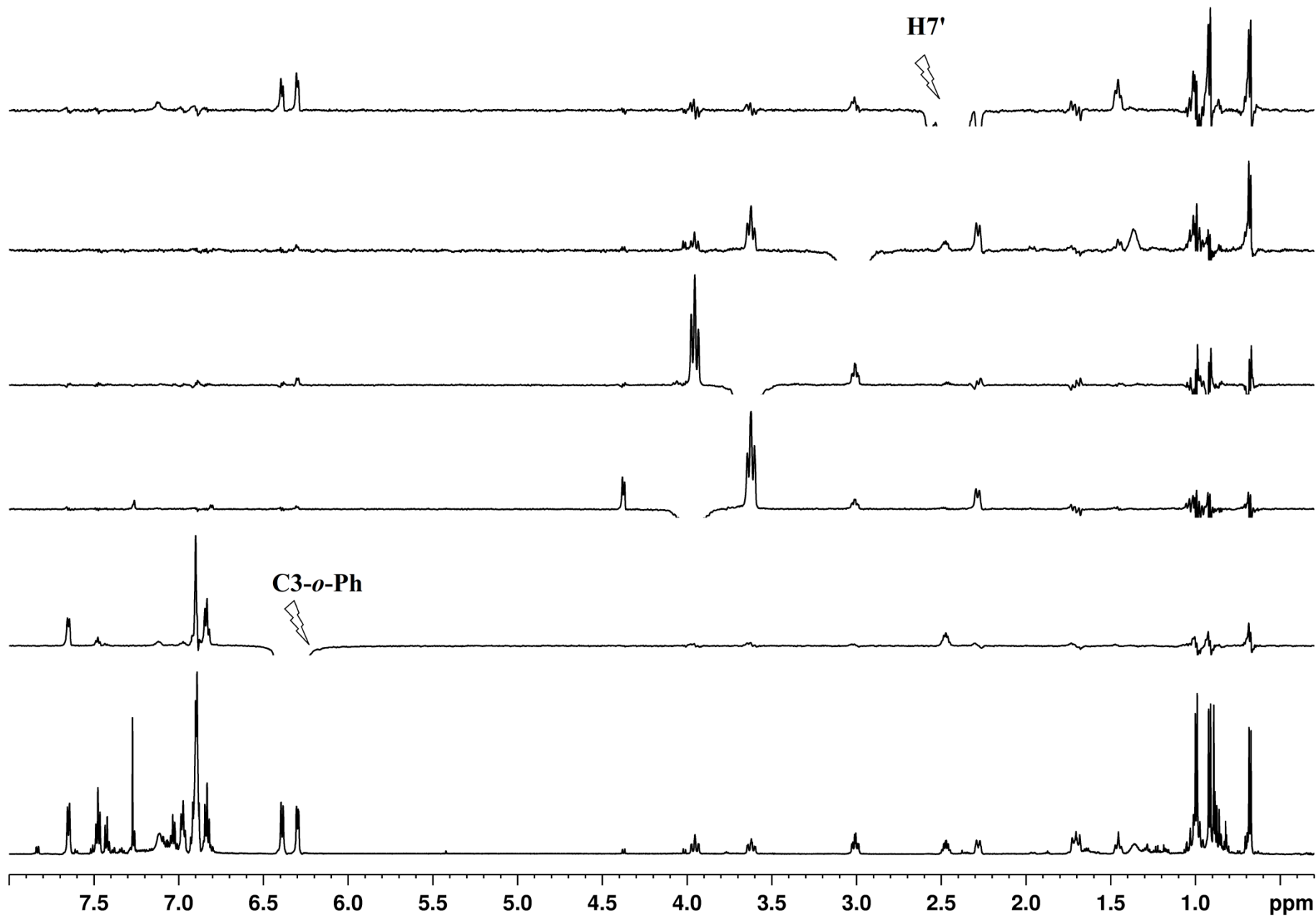


Figure S11. 1D ^1H and ^1H NOESY NMR spectra of **3a** in CDCl_3 at $T = 303 \text{ K}$.

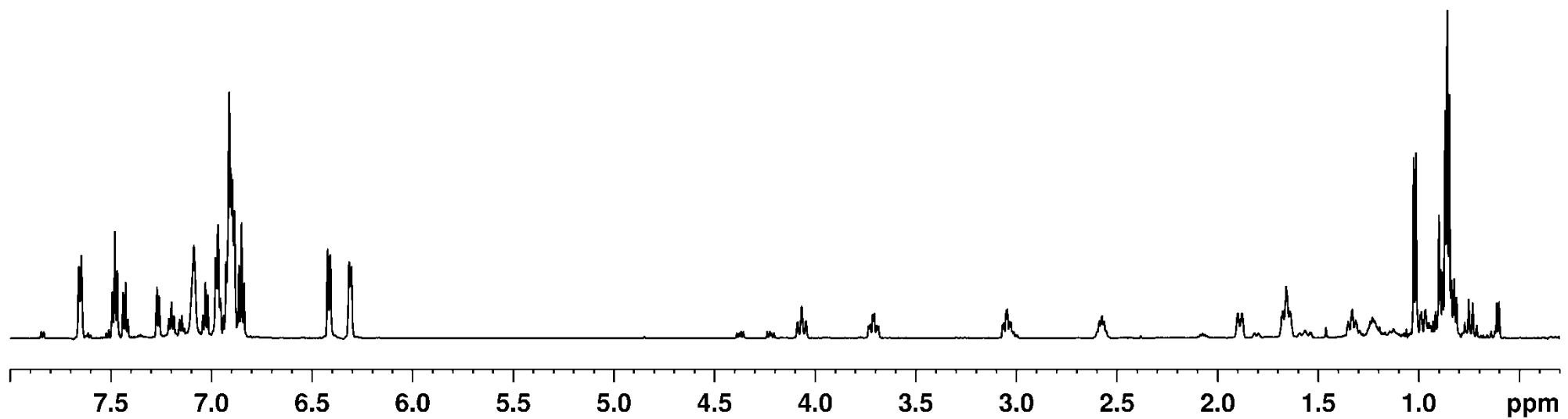
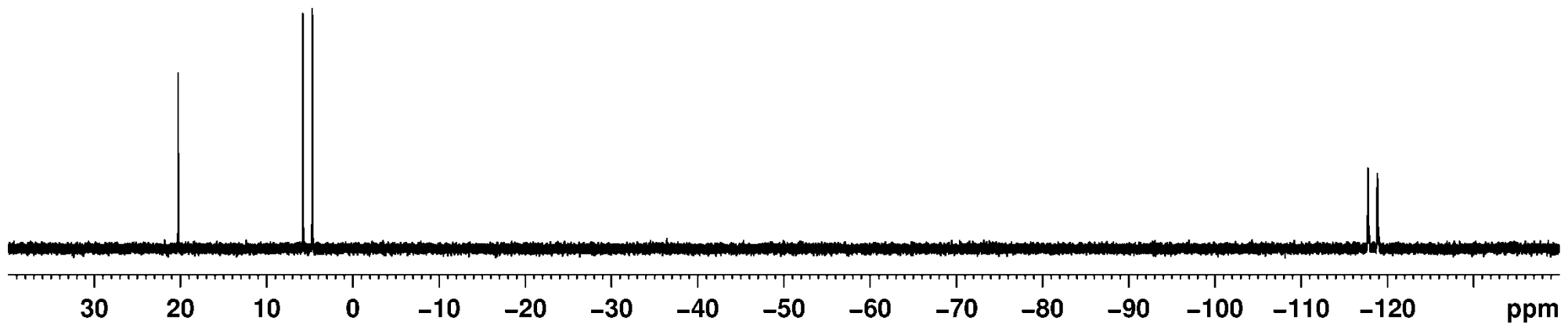


Figure S12. 1D ^1H and $^{31}\text{P}\{^1\text{H}\}$ NMR spectra of **3b** in CDCl_3 at $T = 303$ K.

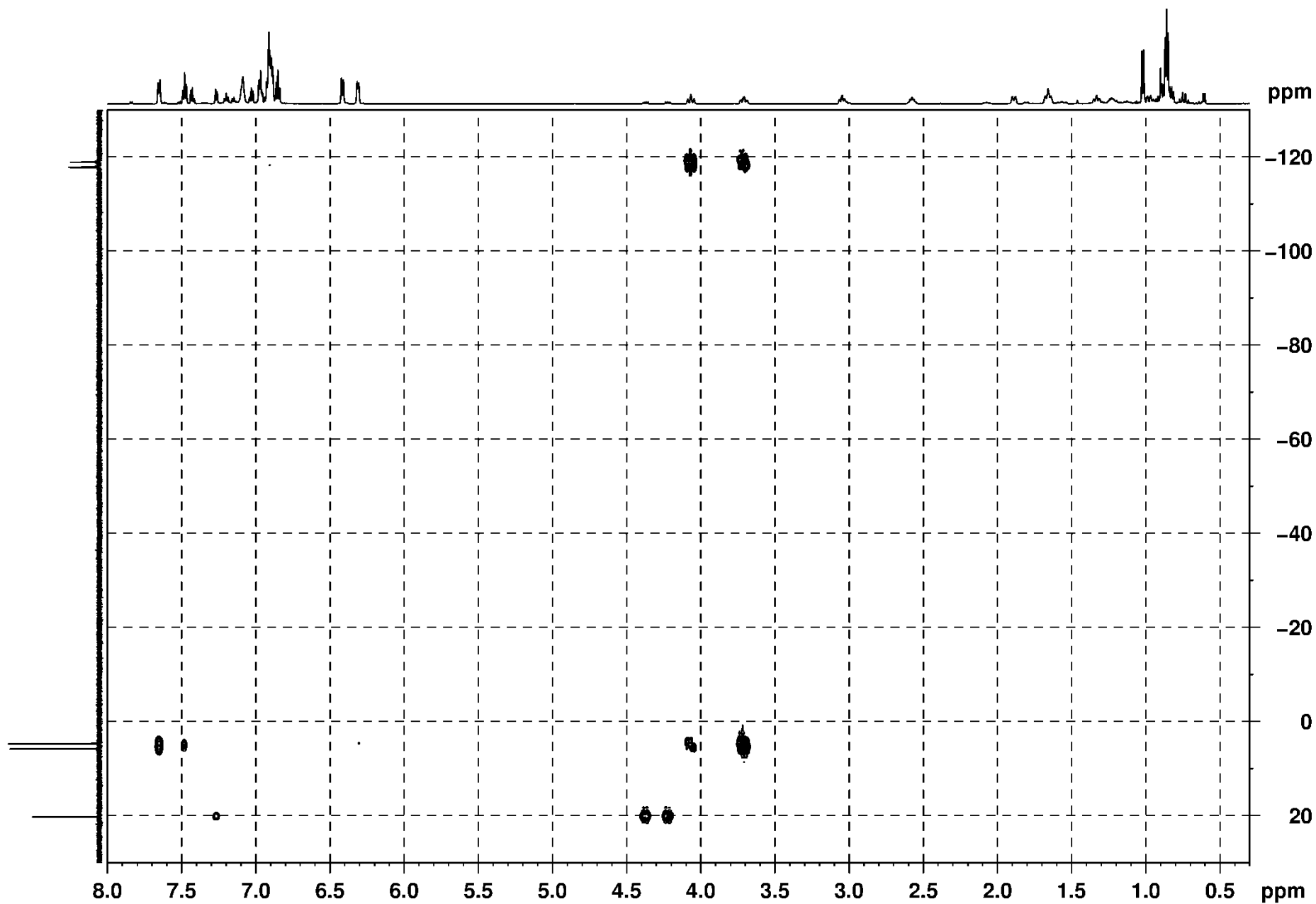


Figure S13. 2D ^1H - ^{31}P HMBC NMR spectrum of **3b** in CDCl_3 at $T = 303$ K.

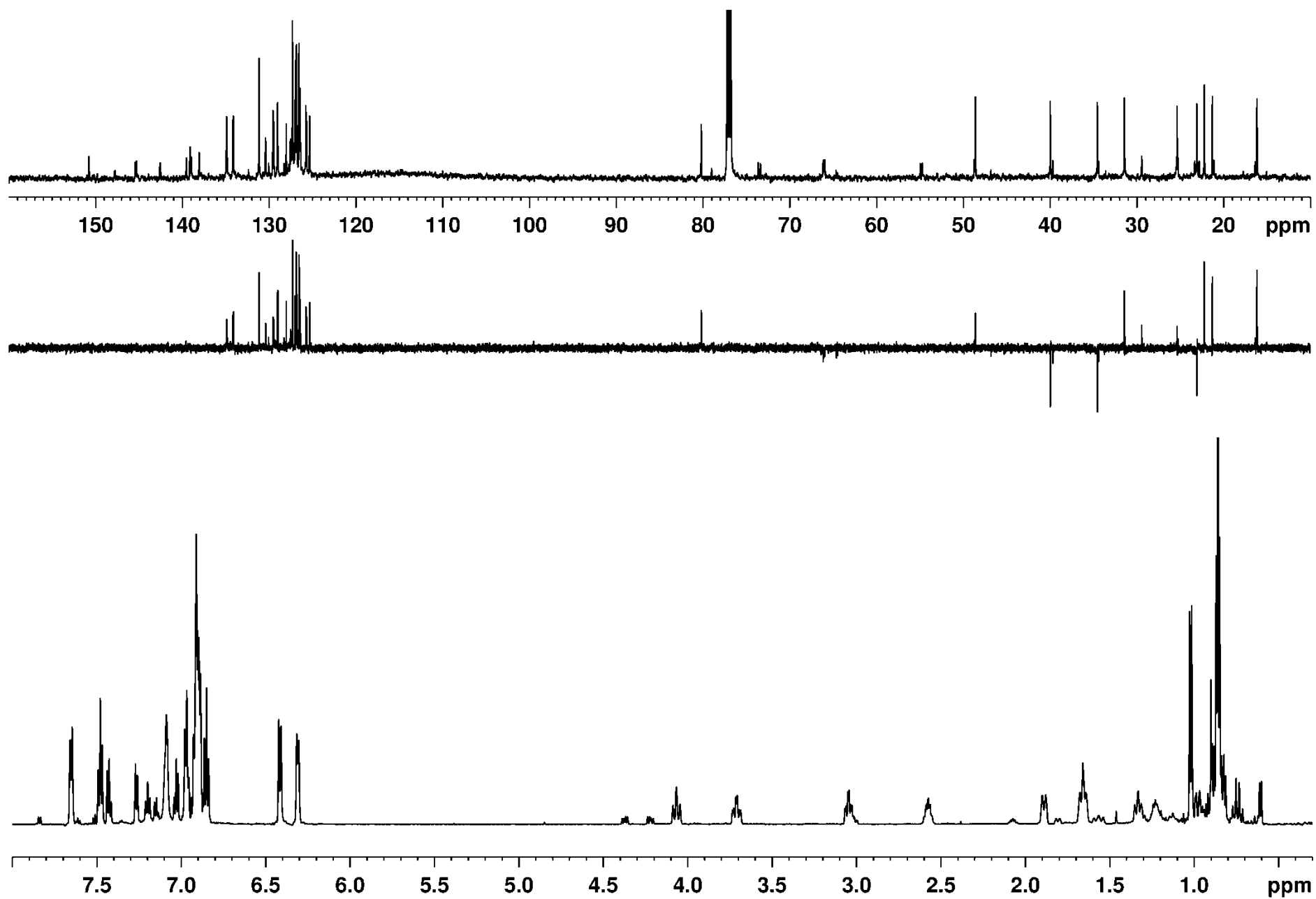


Figure S14. 1D ¹H, ¹³C DEPT and ¹³C{¹H} NMR spectra of **3b** in CDCl₃ at T = 303 K.

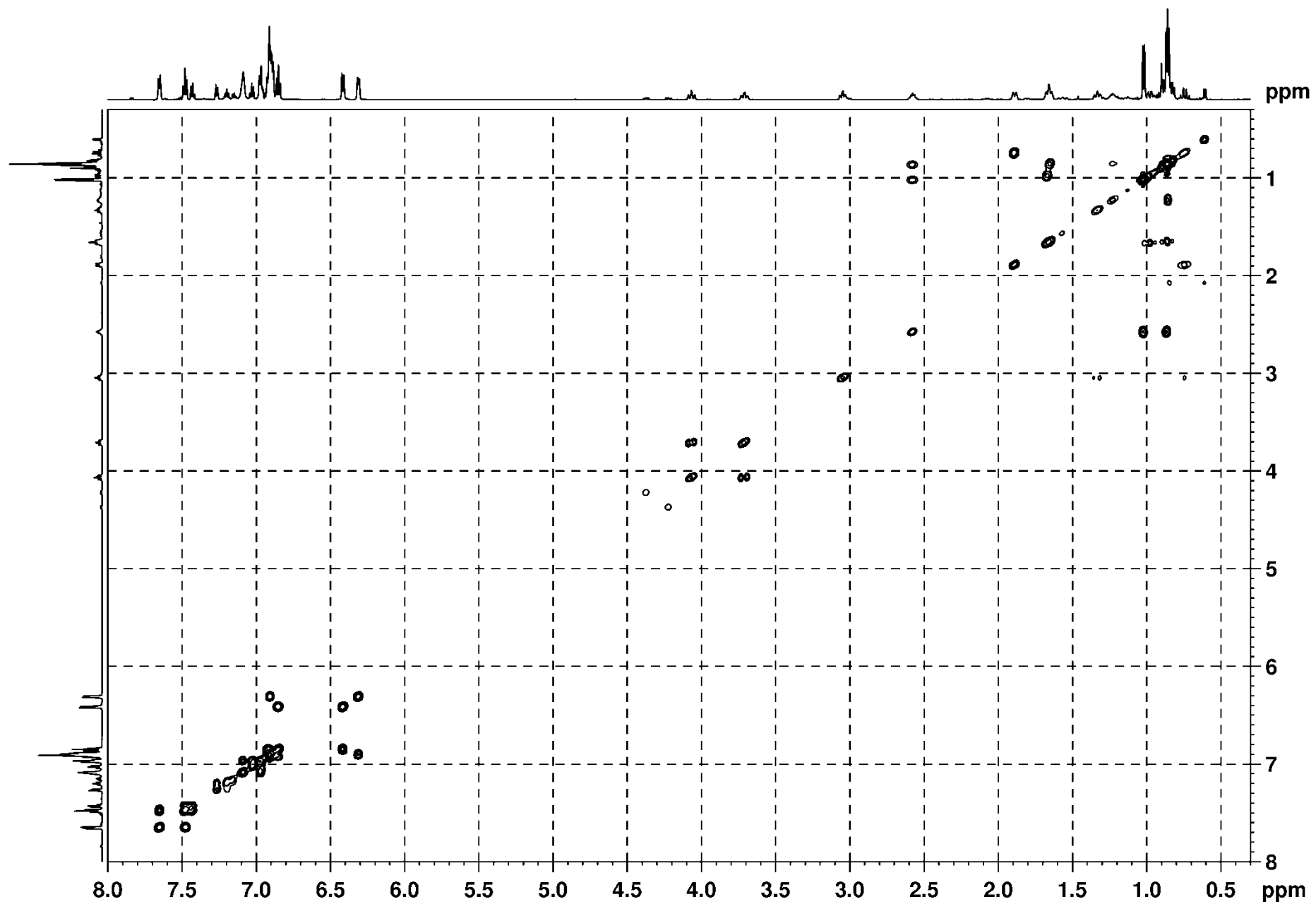


Figure S15. 2D ^1H - ^1H COSY NMR spectrum of **3b** in CDCl_3 at $T = 303$ K.

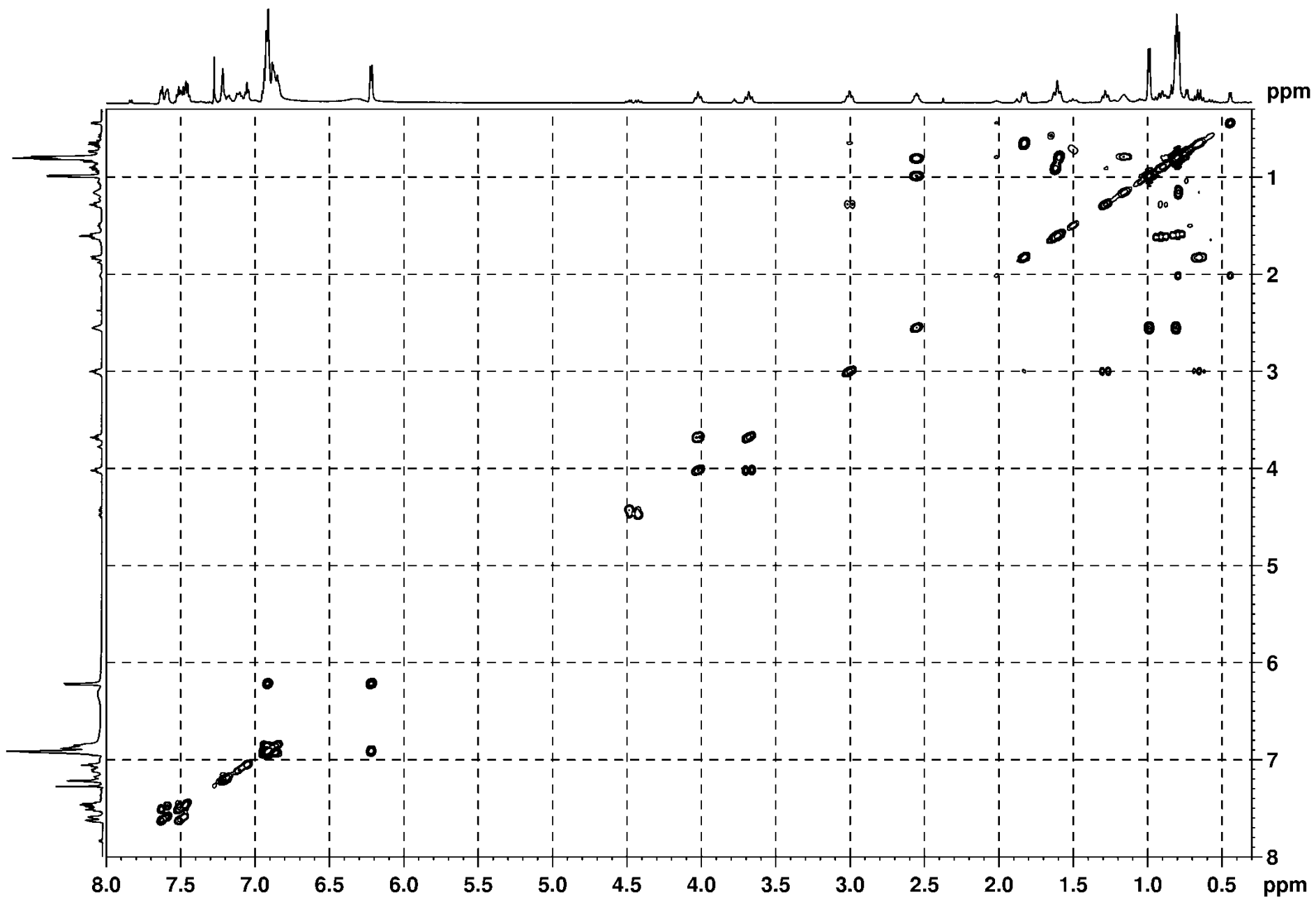


Figure S16. 2D ^1H - ^1H COSY NMR spectrum of **3b** in CDCl_3 at $T = 233\text{ K}$.

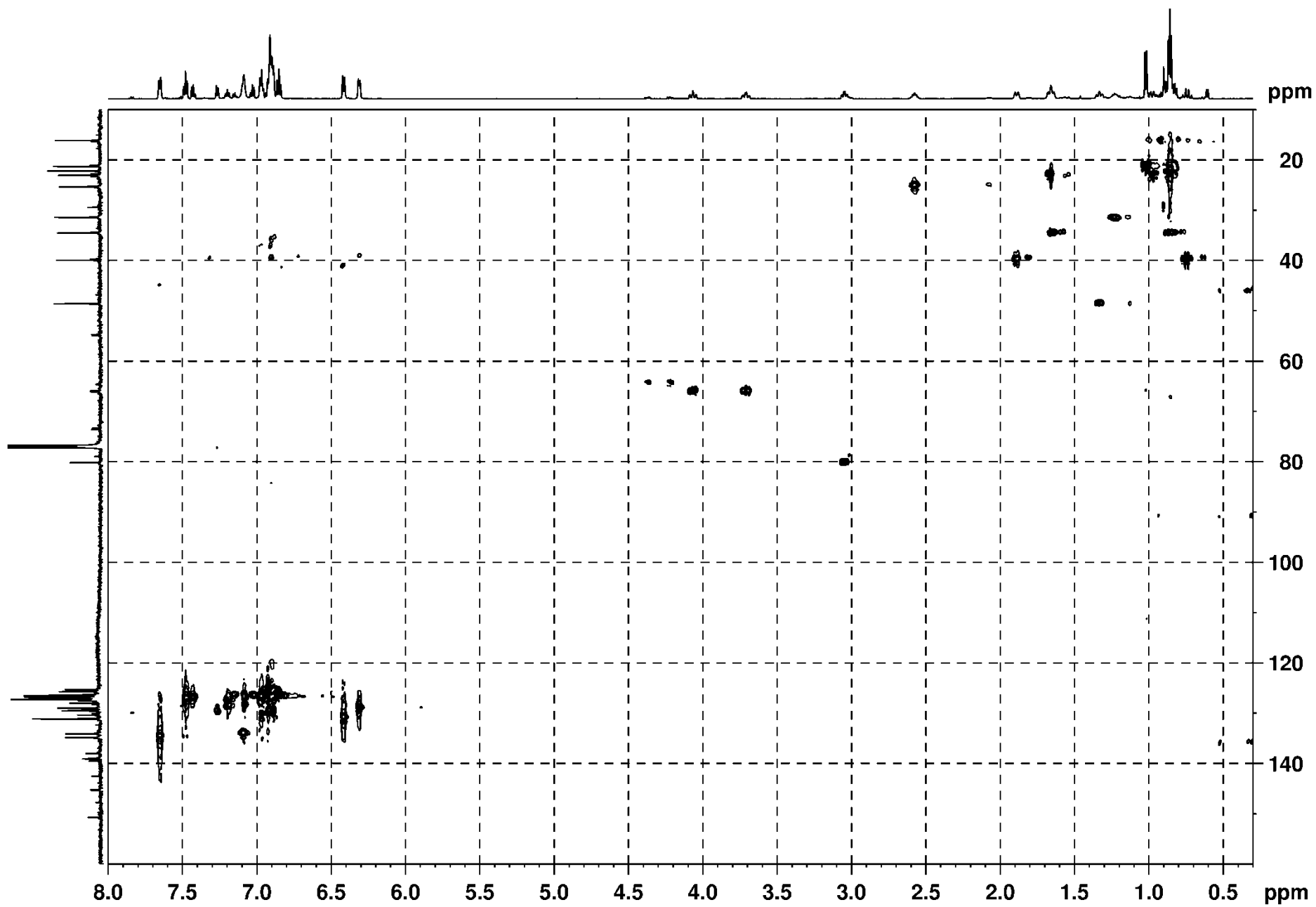


Figure S17. 2D ^1H - ^{13}C HSQC NMR spectrum of **3b** in CDCl_3 at $T = 303$ K.

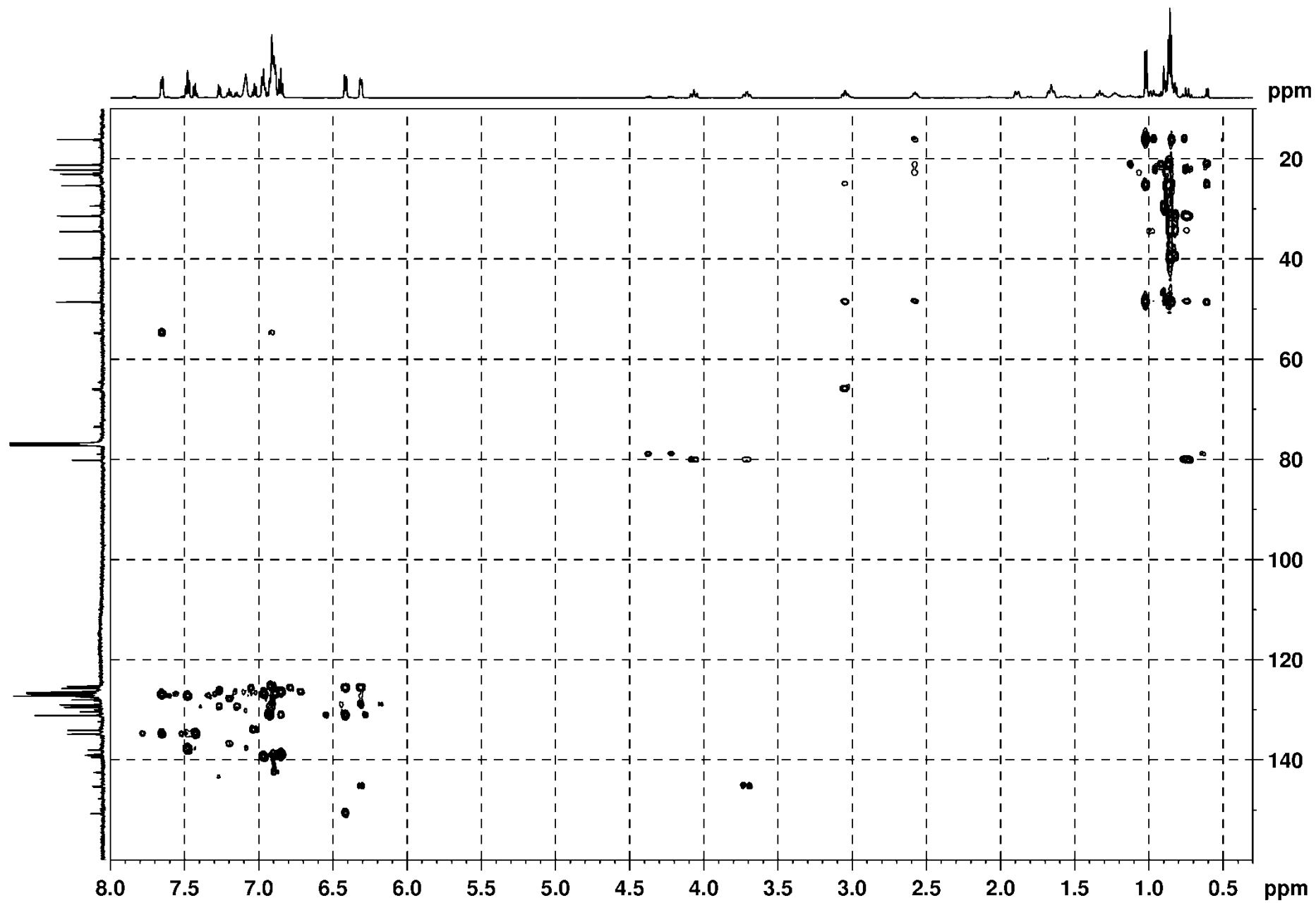


Figure S18. 2D ^1H - ^{13}C HMBC NMR spectrum of **3b** in CDCl_3 at $T = 303$ K.

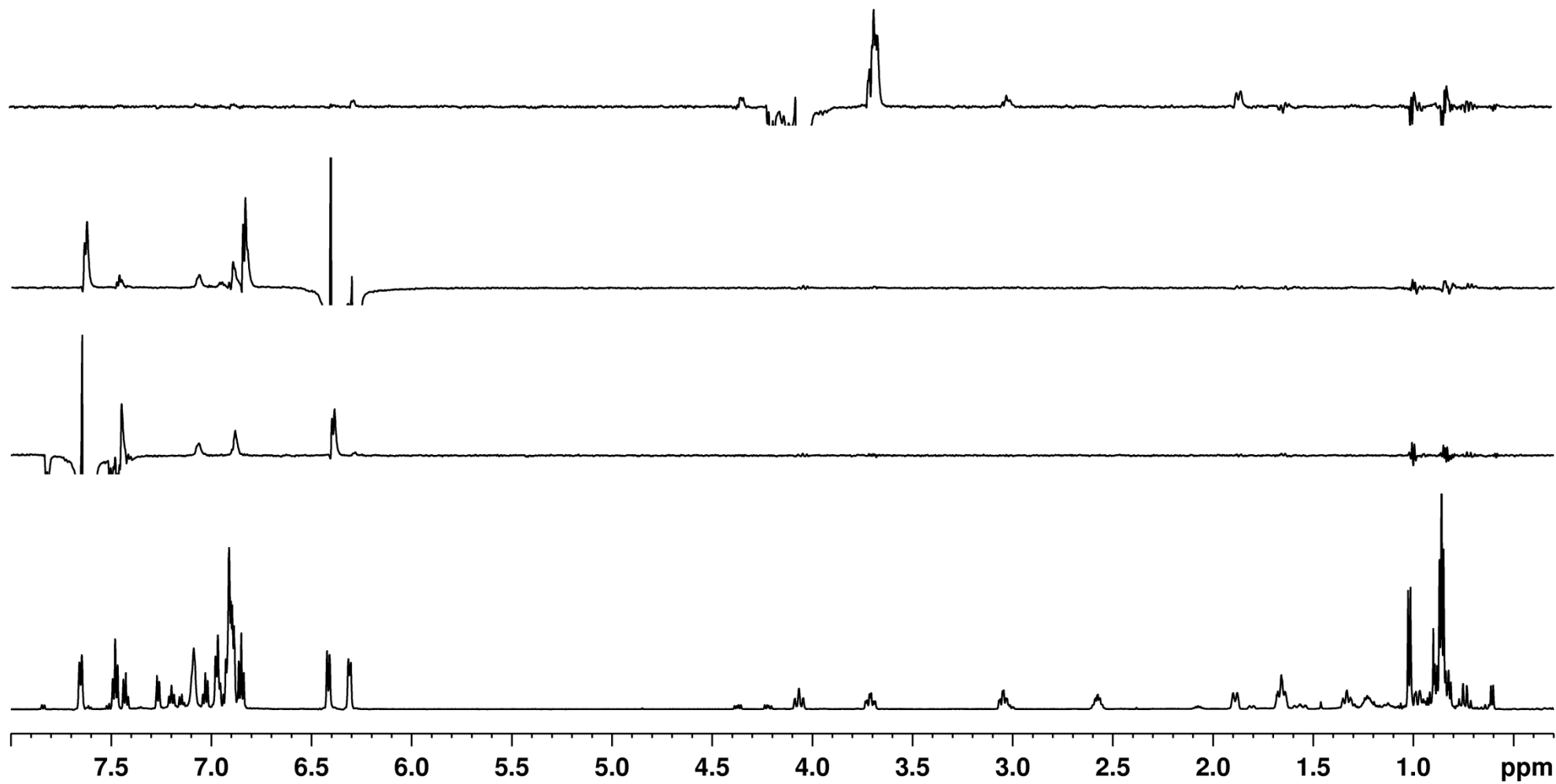


Figure S19. 1D ^1H and ^1H NOESY NMR spectra of **3b** in CDCl_3 at $T = 303 \text{ K}$.

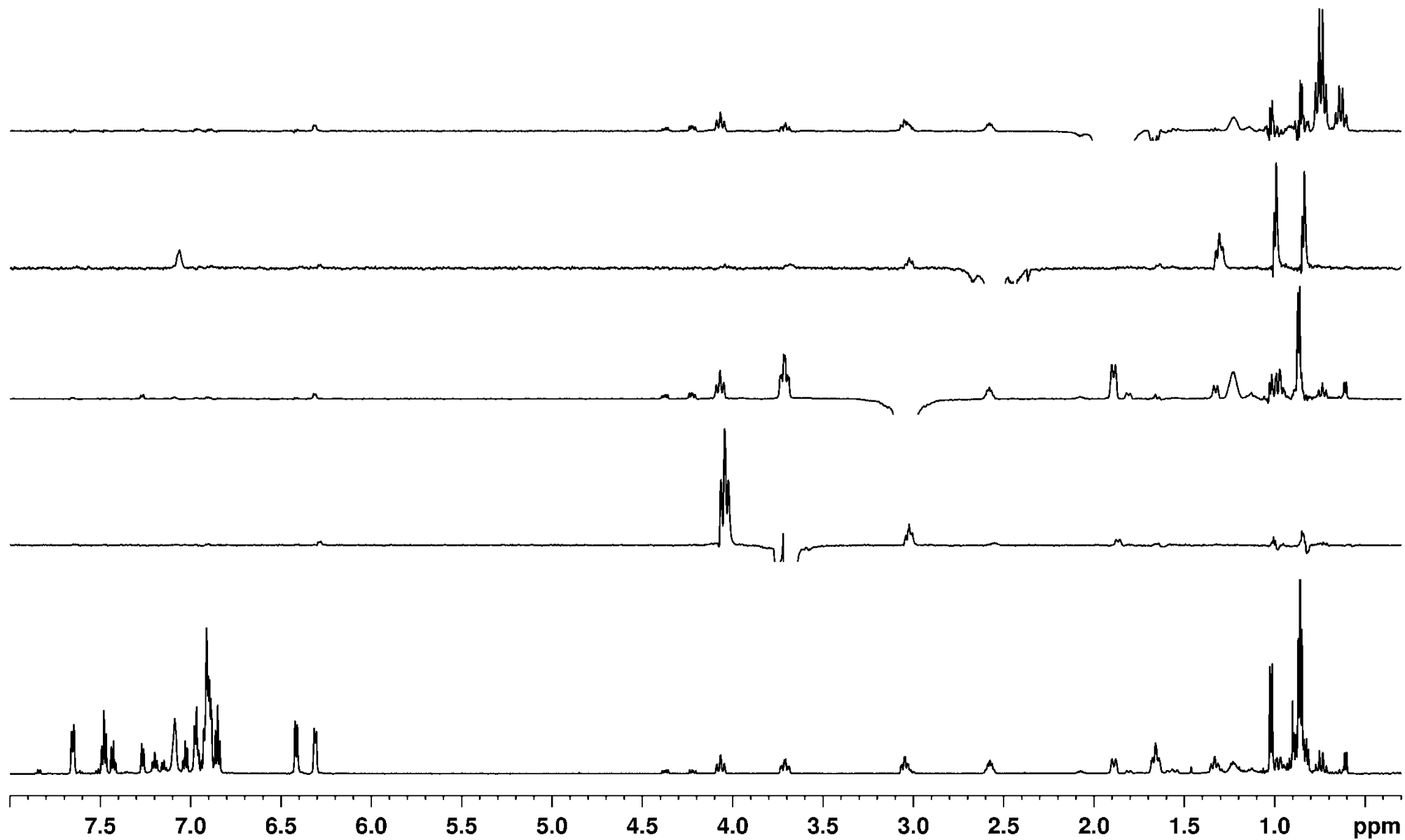


Figure S20. 1D ¹H and ¹H NOESY NMR spectra of **3b** in CDCl₃ at T = 303 K.

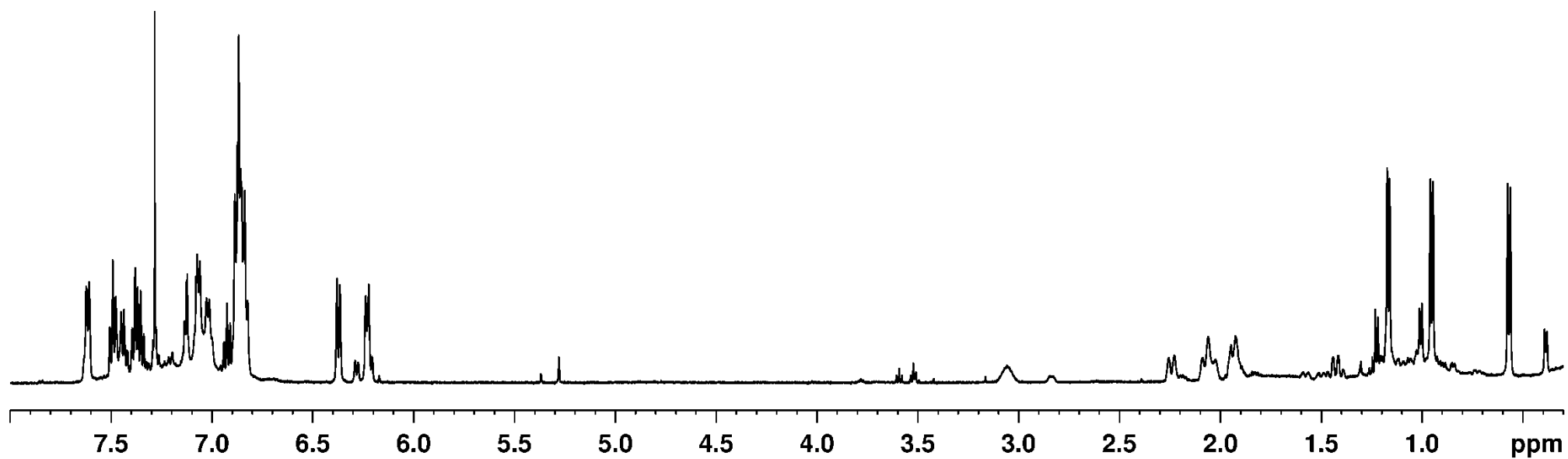
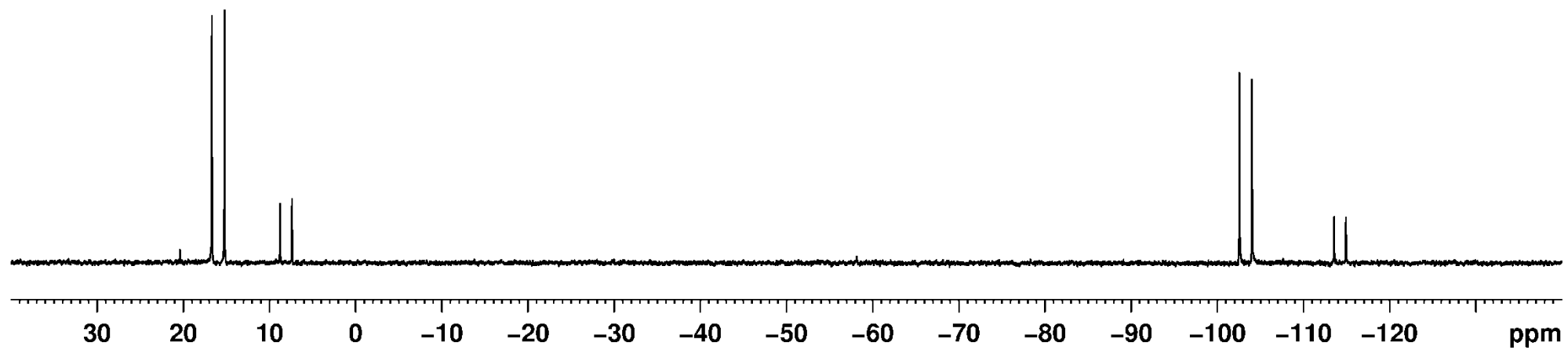


Figure S21. 1D ^1H and $^{31}\text{P}\{^1\text{H}\}$ NMR spectra of **5a** and **5b** in CDCl_3 at $T = 303\text{ K}$.

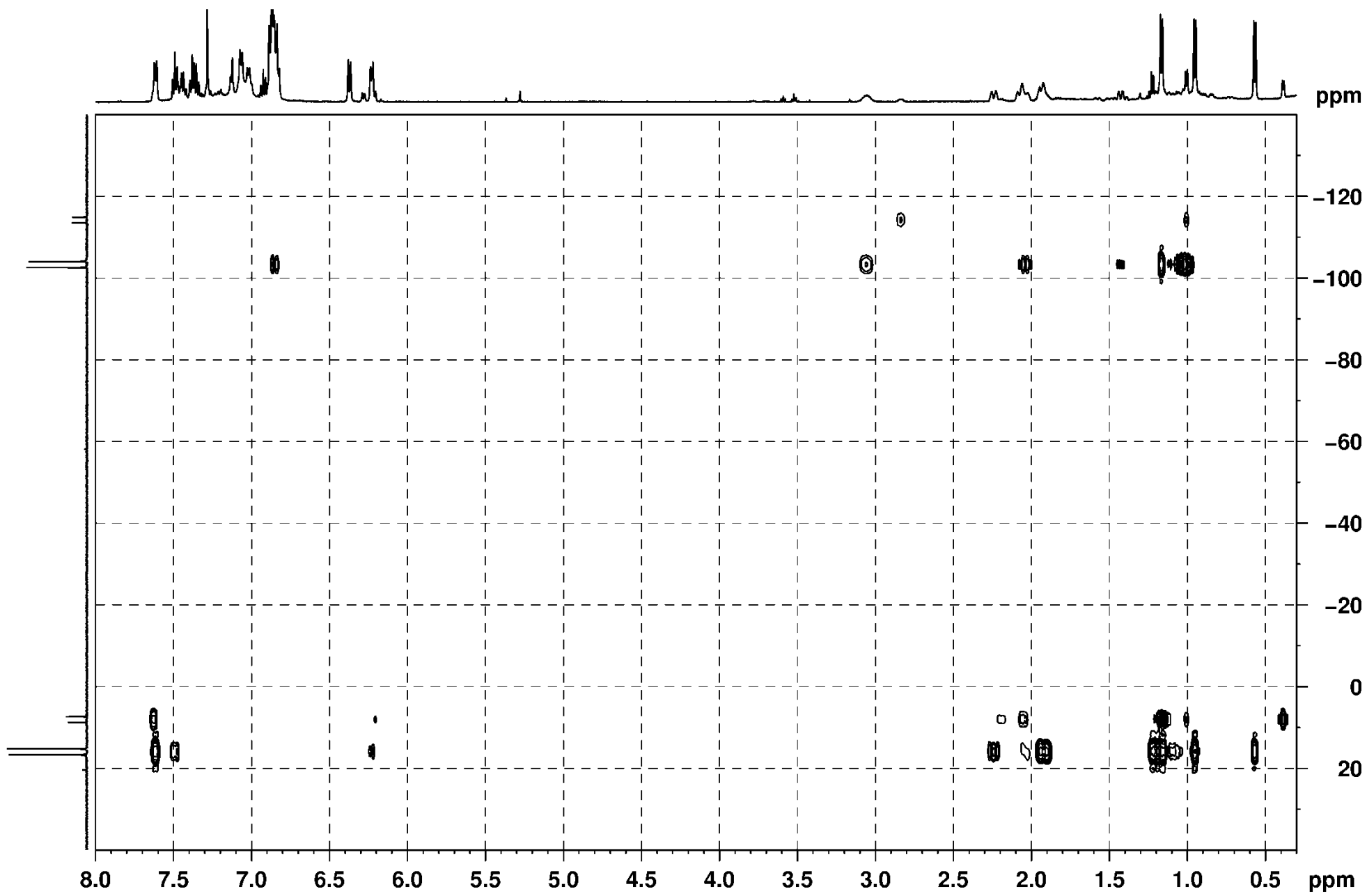


Figure S22. 2D ^1H - ^{31}P HMBC NMR spectrum of **5a** and **5b** in CDCl_3 at $T = 303$ K.

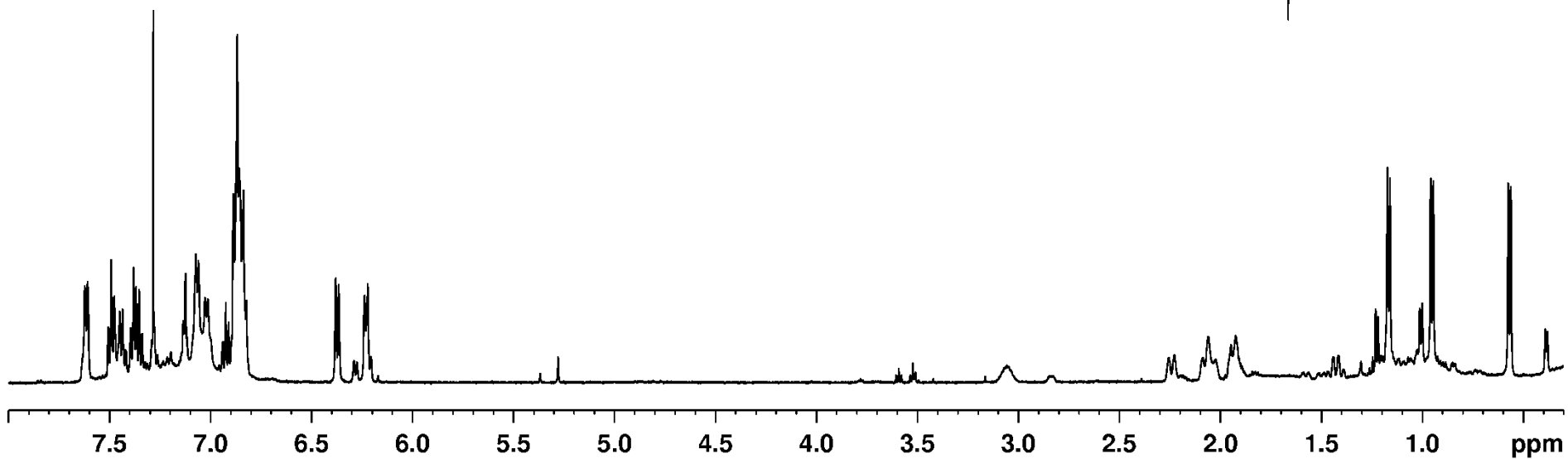
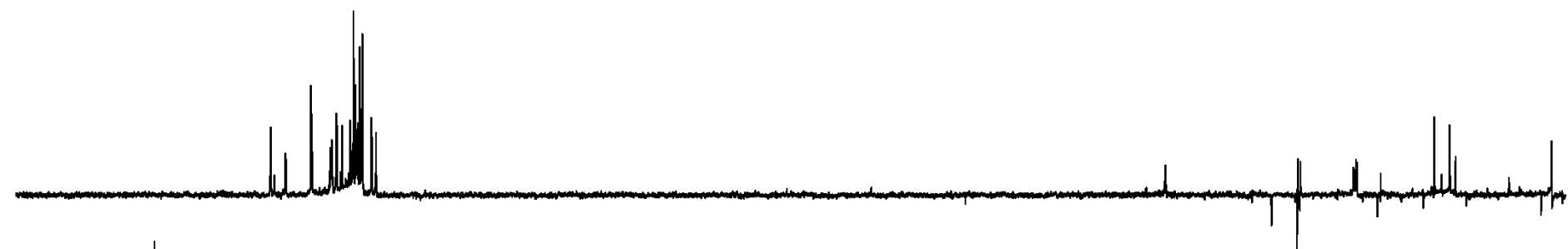
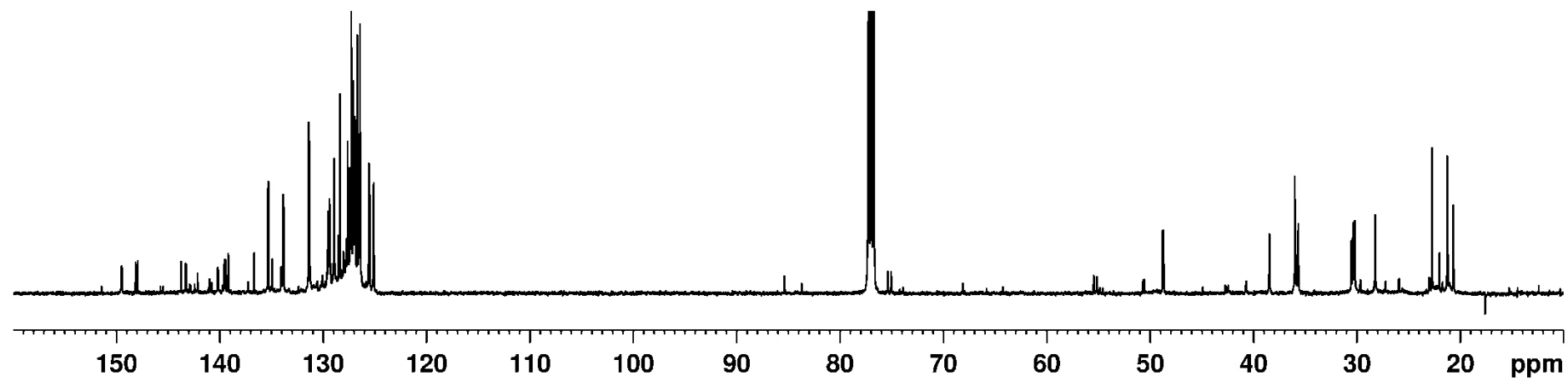


Figure S23. 1D ^1H , ^{13}C DEPT and $^{13}\text{C}\{^1\text{H}\}$ NMR spectra of **5a** and **5b** in CDCl_3 at $T = 303$ K.

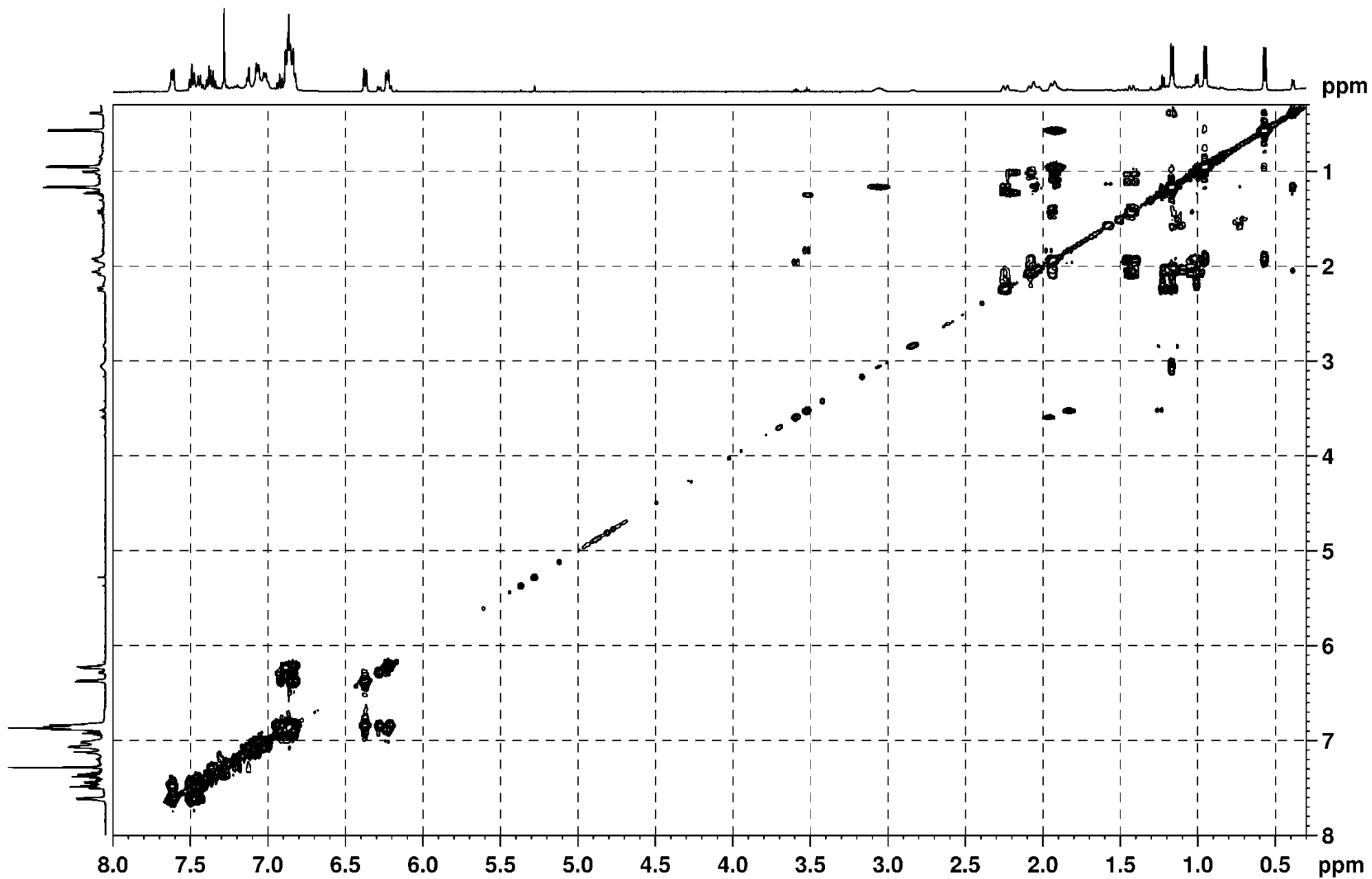


Figure S24. 2D ^1H - ^1H COSY NMR spectrum of **5a** and **5b** in CDCl_3 at $T = 303$ K.

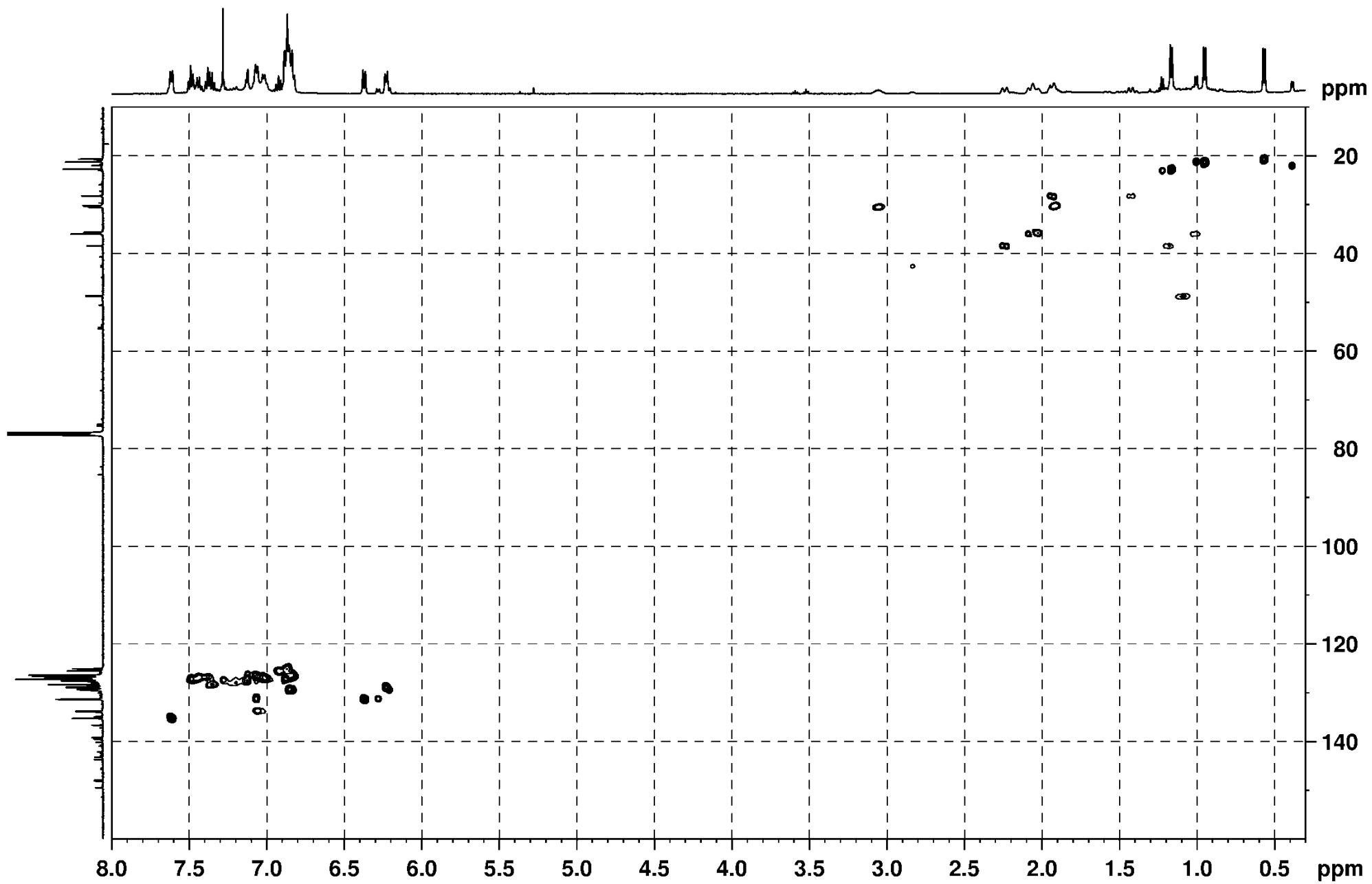


Figure S25. 2D ^1H - ^{13}C HSQC NMR spectrum of **5a** and **5b** in CDCl_3 at $T = 303$ K.

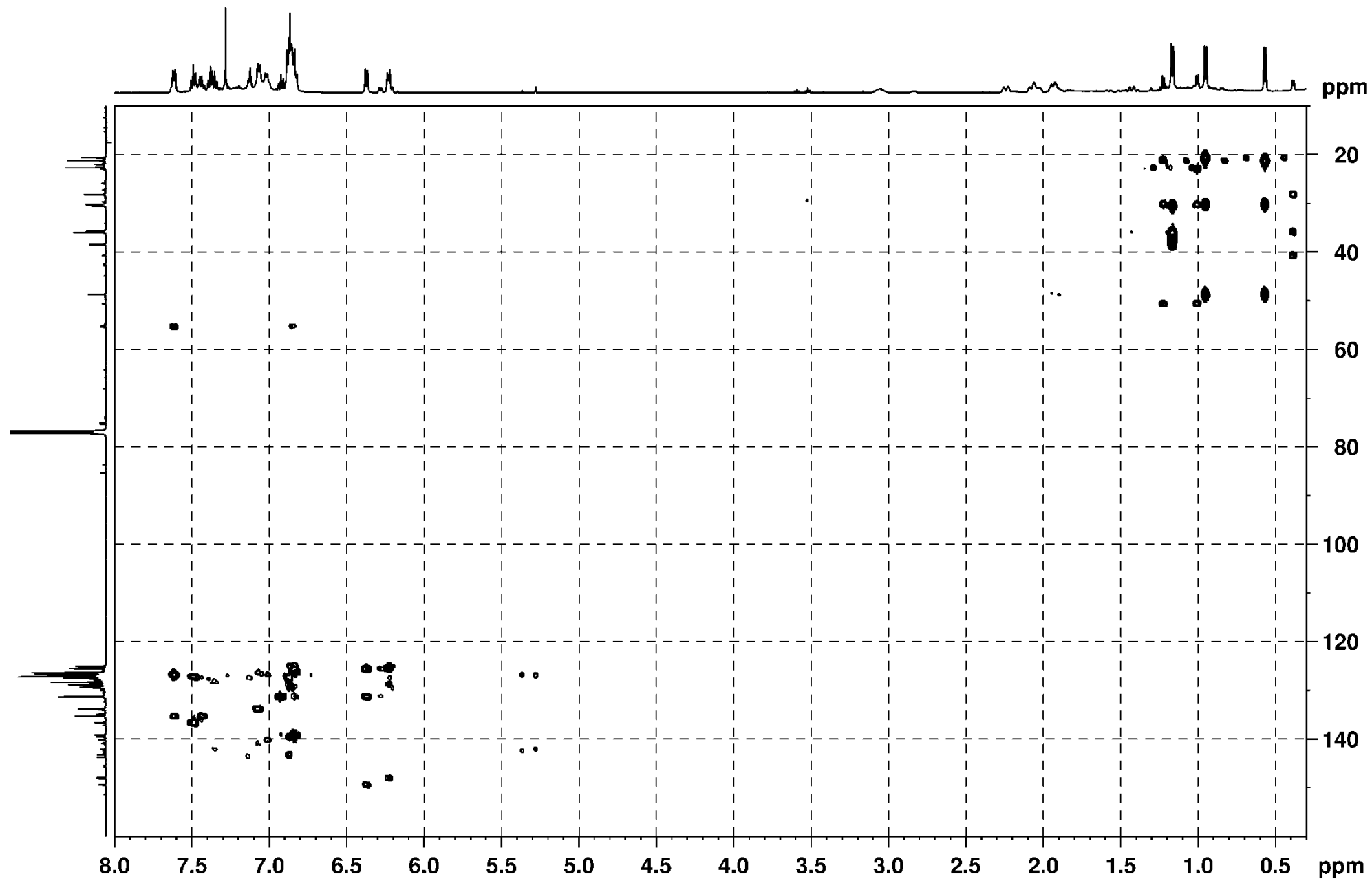


Figure S26. 2D ^1H - ^{13}C HMBC NMR spectrum of **5a** and **5b** in CDCl_3 at $T = 303$ K.

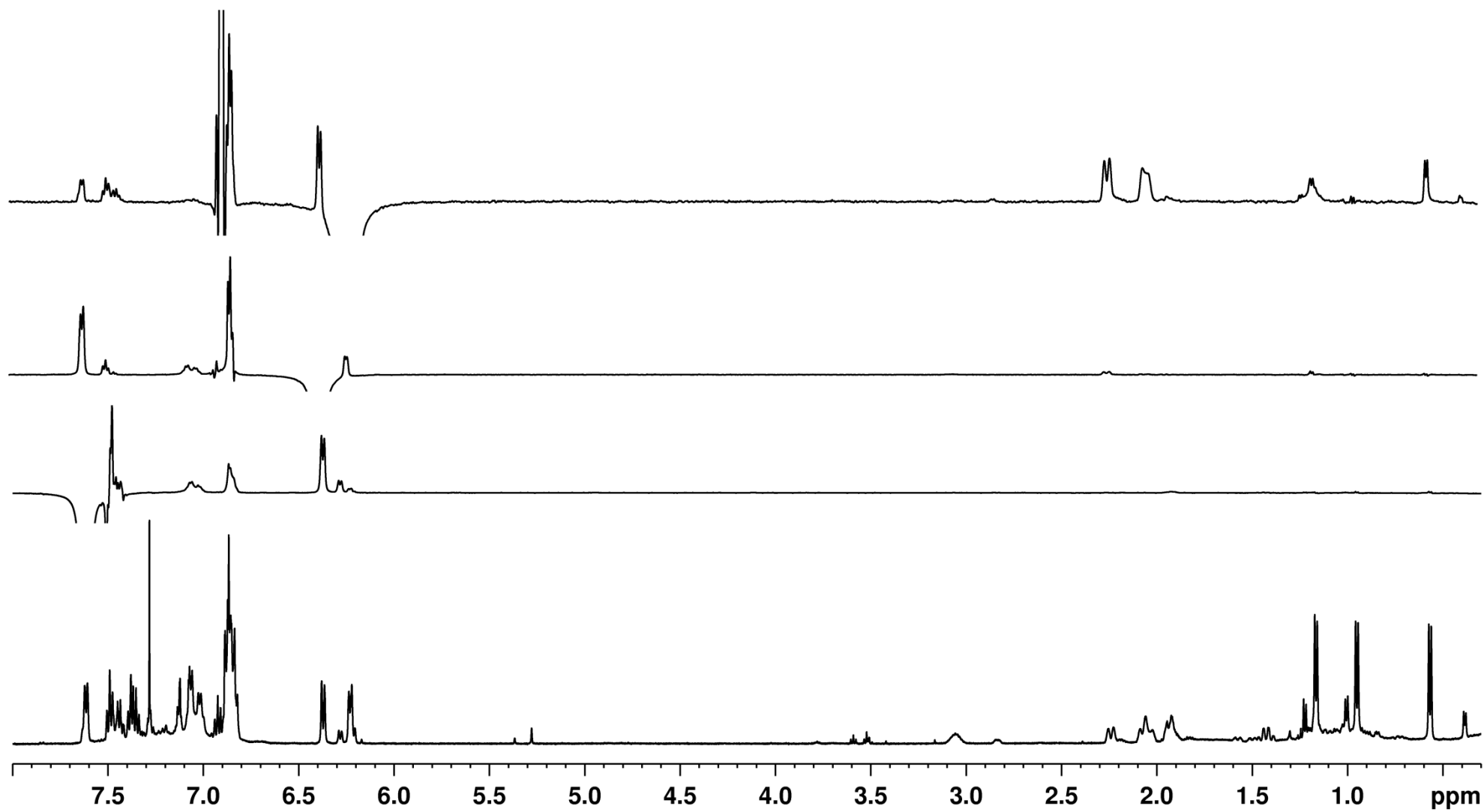


Figure S27. 1D ^1H and ^1H NOESY NMR spectra of **5a** and **5b** in CDCl_3 at $T = 303$ K.

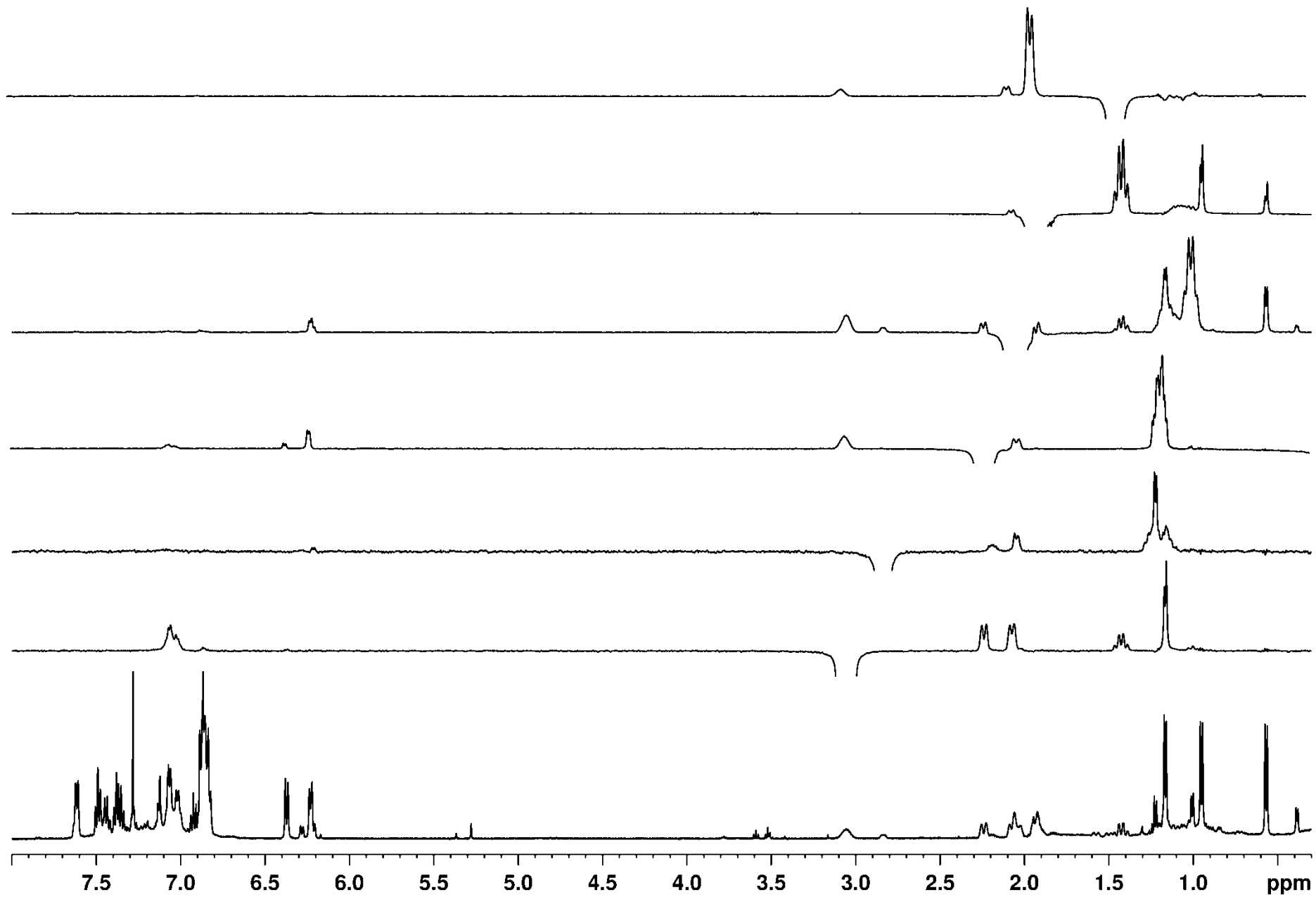


Figure S28. 1D ¹H and ¹H NOESY NMR spectra of **5a** and **5b** in CDCl₃ at T = 303 K.

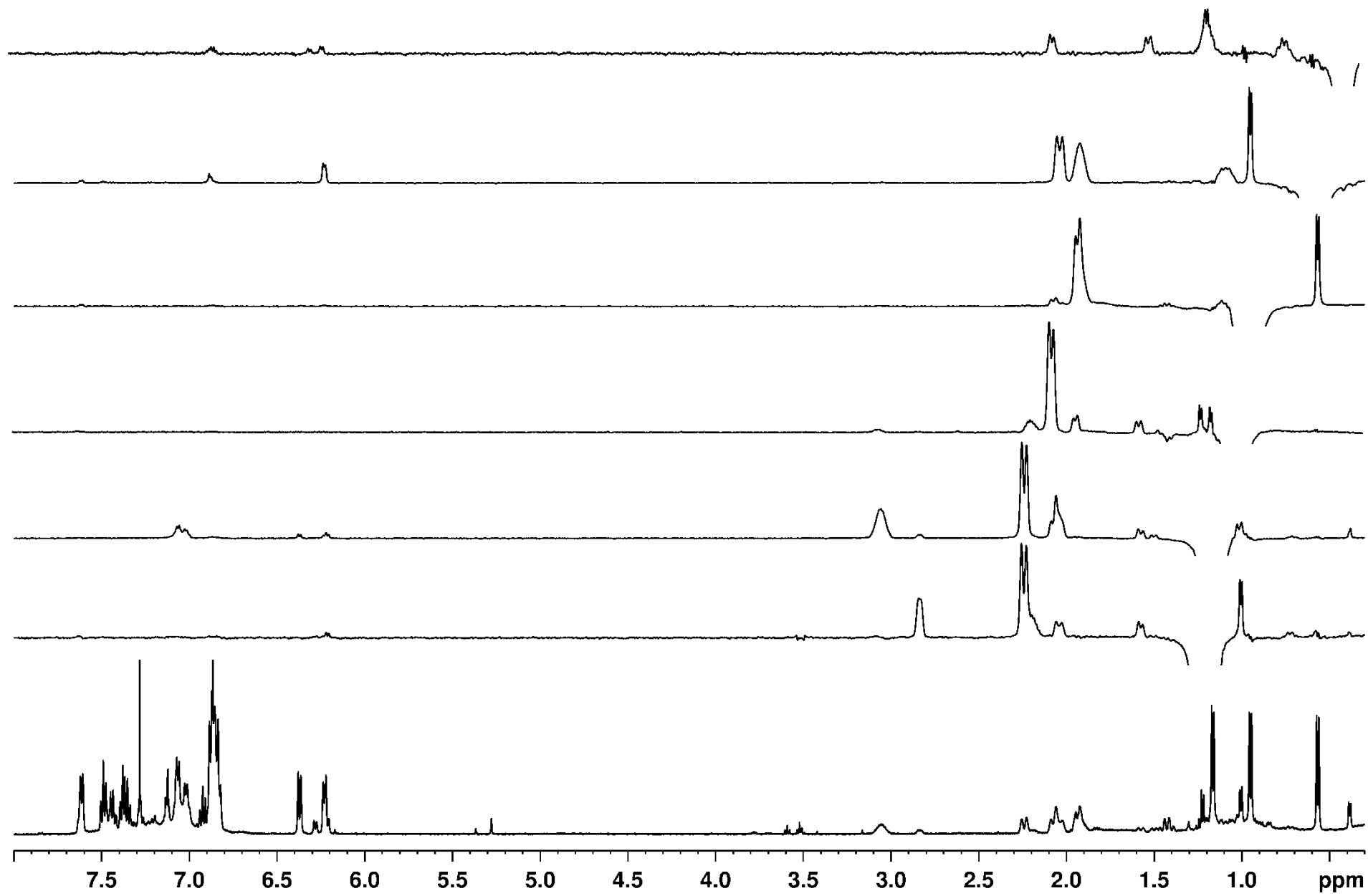


Figure S29. 1D ^1H and ^1H NOESY NMR spectra of **5a** and **5b** in CDCl_3 at $T = 303$ K.

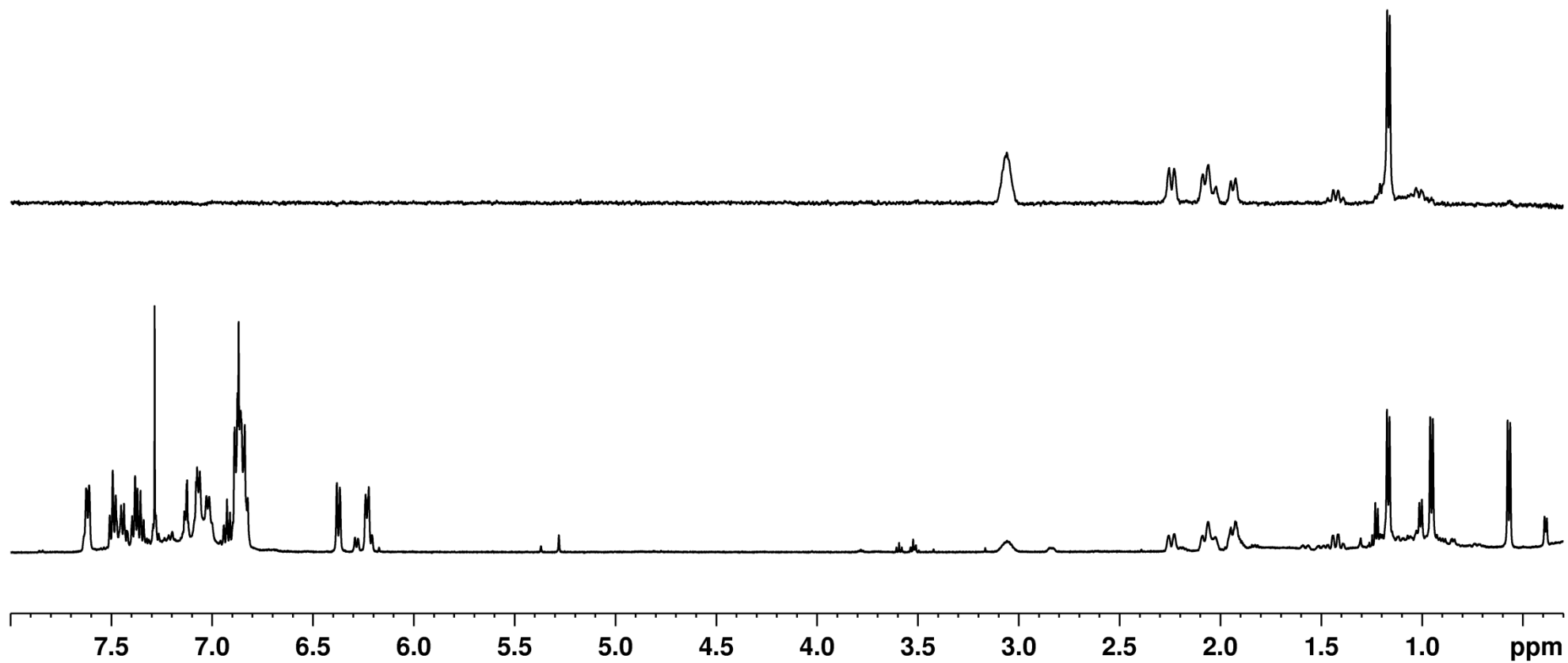


Figure S30. 1D ^1H and ^1H TOCSY NMR spectra of **5a** and **5b** in CDCl_3 at $T = 303\text{ K}$.

X-Ray Structure Determination

The data was collected on a Gemini diffractometer (Rigaku Oxford Diffraction) using Mo-K α radiation ($\lambda = 0.71073 \text{ \AA}$) and ω -scan rotation. Data reduction was performed with CrysAlisPro^[3] including the program SCALE3 ABSPACK for empirical absorption correction. The structure was solved by direct methods (SIR-92)^[4] and the refinement was performed with SHELXL-2018.^[5] Except disordered solvent THF molecules, all non-hydrogen atoms were refined with anisotropic displacement parameters. Hydrogen atoms for methyl substituents and disordered molecules were calculated on idealized positions using the riding model, whereas all other H atoms were located on difference Fourier maps calculated at the final stage of the structure refinement. Structure figures were generated with DIAMOND-4.^[6] Both THF solvent molecules are disordered in the vicinity of a twofold axis. CCDC 1988239 (**5a**) contains the supplementary crystallographic data for this paper. These data can be obtained free of charge via <https://summary.ccdc.cam.ac.uk/structure-summary-form> (or from the Cambridge Crystallographic Data Centre, 12 Union Road, Cambridge CB2 1EZ, UK; fax: (+44)1223-336-033; or deposit@ccdc.cam.ac.uk).

References: see S37

Table S4. Basic crystallographic structure parameters for **5a**.

Molecular formula	C ₄₄ H ₄₄ P ₂ ·THF	Crystal size	0.35 x 0.24 x 0.06 mm ³
Empirical formula	C ₄₈ H ₅₂ OP ₂	Theta range for data collection	2.311 to 30.508°
Formula weight	706.83	Index ranges	-24 ≤ h ≤ 24, -14 ≤ k ≤ 14, -32 ≤ l ≤ 32
Temperature	130(2) K	Reflections collected	26465
Wavelength	0.71073 Å	Independent reflections	12072 [R(int) = 0.0360]
Crystal system	Monoclinic	Completeness to theta = 25.242°	99.9 %
Space group	C2	Absorption correction	Semi-empirical from equivalents
Unit cell dimensions	a = 17.2172(4) Å b = 10.3390(3) Å c = 22.6719(5) Å β = 101.889(2)°	Max. and min. transmission	1.00000 and 0.99370
Volume	3949.2(2) Å ³	Refinement method	Full-matrix least-squares on F ²
Z	4	Data / restraints / parameters	12072 / 39 / 590
Density (calculated)	1.189 Mg/m ³	Goodness-of-fit on F ²	1.006
Absorption coefficient	0.146 mm ⁻¹	Final R indices [I > 2σ(I)]	R1 = 0.0524, wR2 = 0.1224
F(000)	1512	R indices (all data)	R1 = 0.0745, wR2 = 0.1356
		Absolute structure parameter	-0.01(3)
		Residual electron density	0.531 and -0.387 e·Å ⁻³

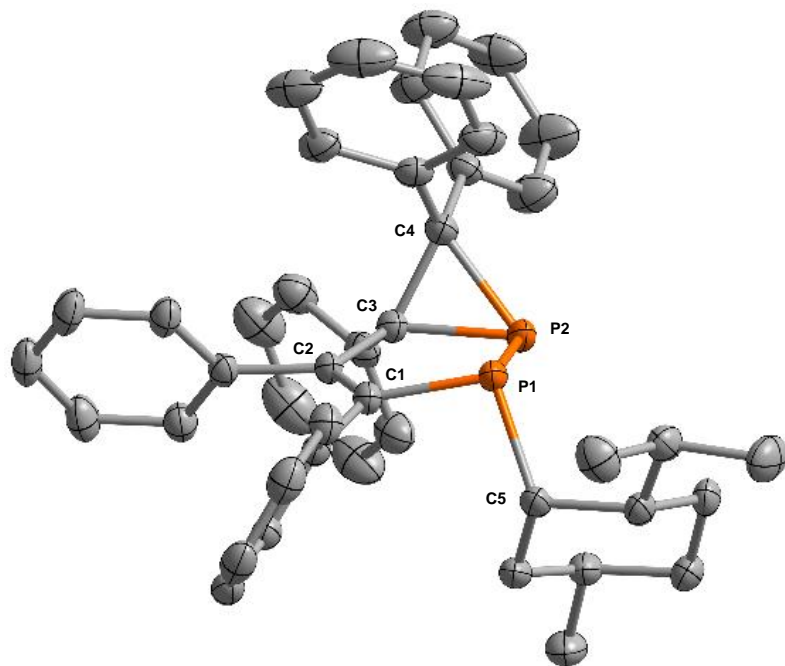


Figure S31. Molecular structure of 2-((+)-neomenthyl)-3,4,5,6,6-pentaphenyl-1,2-(P1_RP2_RC3_S)-diphosfabicyclo[3.1.0]hex-3-ene (**5a**). Hydrogen atoms are omitted for clarity. Configuration of chiral atoms in the five-membered ring: P1:(*R*), P2:(*R*), C3:(*S*). Selected bond lengths [Å] and angles [°]: P1-C1 1.818(3); P1-C5 1.888(3); P1-P2 2.194(1); P2-C4 1.877(3); P2-C3 1.879(3); C1-C2 1.354(4); C2-C3 1.513(4); C3-C4 1.554(4); C1-P1-C5 99.9(1); C1-P1-P2 93.4(1); C4-P2-C3 48.9(1); C4-P2-P1 100.8(1); C3-P2-P1 94.4(1).

A crystal structure analysis of **5a** showed that only one diastereomer was obtained with the neomenthyl group in an *anti* orientation to the 3-membered P2-C3-C4(Ph₂) fragment. Compound **5a** crystallizes in the monoclinic space group *C*₂ with a Flack parameter of -0.01(3). There are 6 chiral centers in **5a**, each phosphorus atom has a typical pyramidal environment and the menthyl fragment has the configuration of (+)-neomenthol or (1*S*,2*S*,5*R*)-2-isopropyl-5-methylcyclohexanol.

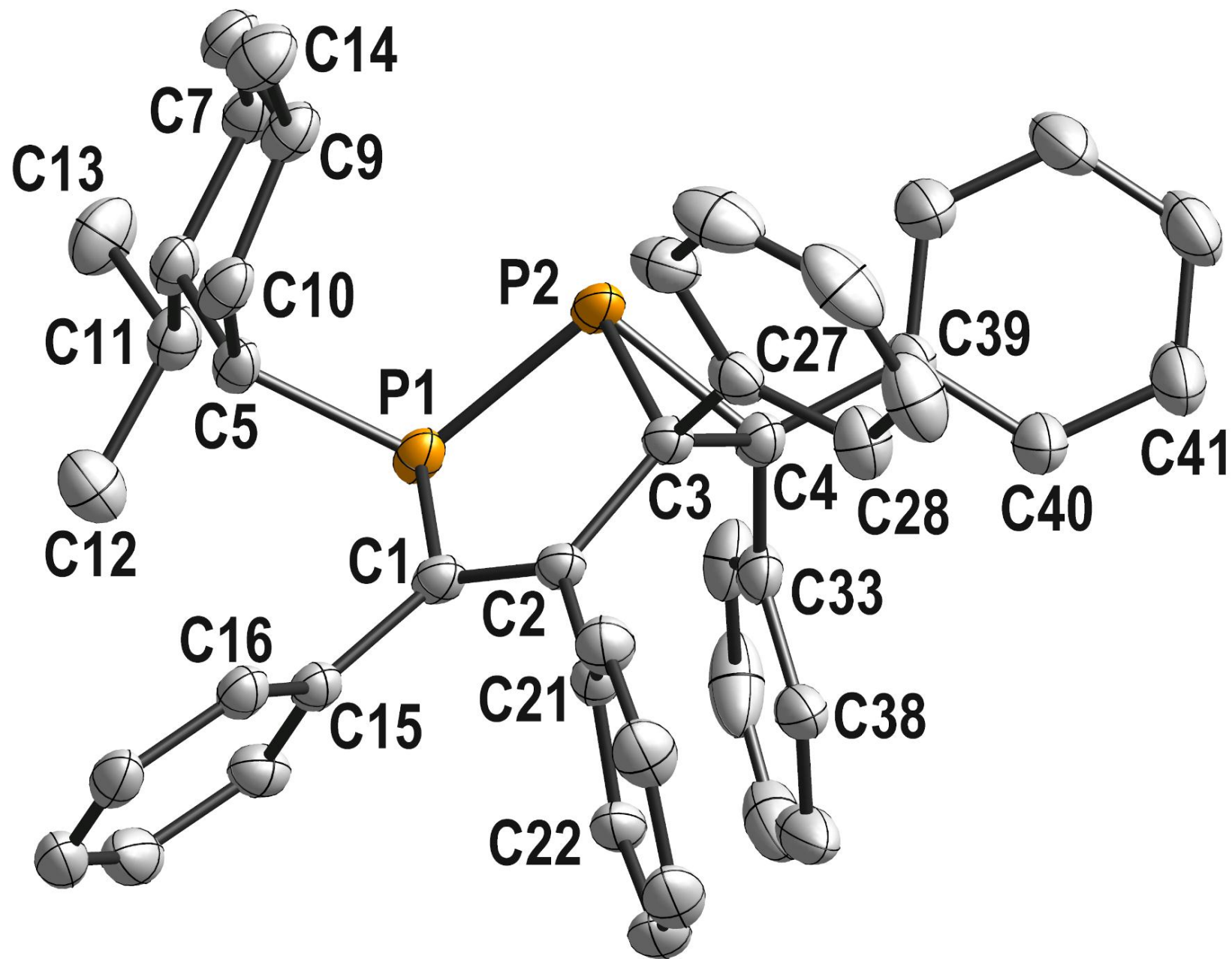


Figure S32. Atom-labeling scheme of **5a**. Displacement ellipsoids are drawn at the 50% probability level and H atoms are omitted for clarity.

References

- (1) Frisch, M. J.; Trucks, G. W.; Schlegel, H. B.; Scuseria, G. E.; Robb, M. A.; Cheeseman, J. R.; Montgomery, J. A., Jr.; Vreven, T.; Kudin, K. N.; Burant, J. C.; Millam, J. M.; Iyengar, S. S.; Tomasi, J.; Barone, V.; Mennucci, B.; Cossi, M.; Scalmani, G.; Rega, N.; Petersson, G. A.; Nakatsuji, H.; Hada, M.; Ehara, M.; Toyota, K.; Fukuda, R.; Hasegawa, J.; Ishida, M.; Nakajima, T.; Honda, Y.; Kitao, O.; Nakai, H.; Klene, M.; Li, X.; Knox, J. E.; Hratchian, H. P.; Cross, J. B.; Adamo, C.; Jaramillo, J.; Gomperts, R.; Stratmann, R. E.; Yazyev, O.; Austin, A. J.; Cammi, R.; Pomelli, C.; Ochterski, J. W.; Ayala, P. Y.; Morokuma, K.; Voth, G. A.; Salvador, P.; Dannenberg, J. J.; Zakrzewski, V. G.; Dapprich, S.; Daniels, A. D.; Strain, M. C.; Farkas, O.; Malick, D. K.; Rabuck, A. D.; Raghavachari, K.; Foresman, J. B.; Ortiz, J. V.; Cui, Q.; Baboul, A. G.; Clifford, S.; Cioslowski, J.; Stefanov, B. B.; Liu, G.; Liashenko, A.; Piskorz, P.; Komaromi, I.; Martin, R. L.; Fox, D. J.; Keith, T.; Al-Laham, M. A.; Peng, C. Y.; Nanayakkara, A.; Challacombe, M.; Gill, P. M. W.; Johnson, B.; Chen, W.; Wong, M. W.; Gonzalez, C.; Pople, J. A. *Gaussian 03, Revision B.04*; Gaussian, Inc., Pittsburgh, PA, 2003.
- (2) Latypov, Sh.K.; Polyancev, F.M.; Yakhvarov, D.G.; Sinyashin, O.G. Quantum Chemical Calculations of ^{31}P NMR Chemical Shifts: Scopes and Limitations. *Phys. Chem. Chem. Phys.* **2015**, *17*, 6976–6987.
- (3) CrysAlisPro: Data reduction software package, Rigaku Oxford Diffraction, Oxford, UK.
- (4) SIR92: A. Altomare, G. Cascarano, C. Giacovazzo and A. Guagliardi, *J. Appl. Crystallogr.* 1993, *26*, 343-350
- (5) SHELXL: G. M. Sheldrick, *Acta Cryst.* C71 (2015) 3 – 8
- (6) DIAMOND 4: K. Brandenburg, Crystal Impact GbR, Bonn, Germany